Improving the Patch Transfer Function Approach for Fluid-Structure Modelling in Heavy Fluid

Laurent Maxit, Mathieu Aucejo, Jean-Louis Guyader

Improving the Patch Transfer Function approach for fluid-structure modelling in heavy fluid

L. Maxit, M. Aucejo & J.-L. Guyader

Laboratoire Vibrations-Acoustique
INSA Lyon
25 bis, av. Jean Capelle
69621 Villeurbanne Cedex - France
Tel. +33 4 72 43 80 82
Fax. + 33 4 72 43 87 12
laurent.maxit@insa-lyon.fr

The vibro-acoustic behaviour of elastic structures coupled with cavities filled with a heavy fluid can be modelled by using the Finite Element Method. In order to reduce computing time, the Patch Transfer Function (PTF) approach is used to partition the global problem into different sub-problems. Different types of problem partitioning are studied in this paper. Partitioning outside the near field of structures to reduce the number of patches of the coupling surface for frequencies below the critical frequency is of particular interest. This implies introducing a non standard modal expansion to compute the PTF accurately enough to guarantee the convergence of the PTF method and reduce computation time in comparison to a direct Finite Element resolution. An application on a submarine structure illustrates the interest of this approach.

1 Introduction

The response of elastic structures coupled to water-filled cavities is investigated in this paper. The interaction between a mechanical structure and a heavy fluid is of particular interest, especially in nuclear and naval engineering. In this situation, the structure is strongly influenced by the presence of the surrounding fluid (generally water) [1].

Different numerical methods have been developed in recent decades to model fluid-structure interaction problems. The Finite Element Method (FEM) and the Boundary Element Method (BEM) are the methods most commonly used in industrial contexts. The advantage of these approaches is that they can be applied to any geometry and a wide range of mechanical properties. However, they are generally limited to the low frequency range, although the inexorable increase in computing capacities tends to extend their applicability to higher frequencies. This limitation of frequency has two main causes : (a) the increase in the number of degrees of freedom of the FE model as a function of increasing frequency; (b) the non-symmetric *(u,p)* formulation of the fluid-structure interaction problem prevents the use of classical methods to extract the normal modes. The standard modal method cannot be employed. Moreover, the direct resolution of such systems of equations is very time-consuming. In order to overcome this drawback, different approaches have been proposed in recent decades. Some of them [2-4] have used the normal modes of each uncoupled-subsystem (i.e. in-vacuo modes of the structure and acoustic modes of the cavity with rigid wall). In the case of a heavy fluid, the use of uncoupled modal bases can lead to poor convergence if the coupling between the high order modes of a given subsystem with the low order modes of another system is not considered in the computation. In order to improve the convergence of these modal expansions, the modal basis can be enriched by a set of residual modes defined as the static response of a subsystem (i.e. structure or cavity) to the excitation by a mode shape of the other subsystem [2]. The number of residual modes is therefore equal to the number of normal modes which can limit the approach. Similarly, Tournour et al. [5-6] showed that the effect of modal truncation using the normal modes of a plate and a cavity is critical for the convergence of the method and that convergence can be greatly improved by using pseudostatic corrections for both the structure and the cavity. They also show that using only a pseudostatic correction for the structure is not sufficient to accurately calculate the pressure inside the cavity. Another approach is the use of symmetric variational principles, as done in [7], that can lead to a single field “limit case” formulation. The modes of these “limit cases” can provide basic functions for the structure and the fluid variables, thus leading to a large number of possible modal methods. However, these methods are time-consuming [6]. Other theoretical reduced models [8-10] have been proposed for the linear vibration analysis of bounded fluid-structure systems in low modal density situations. They lead to symmetric reduced matrix systems expressed in terms of generalized coordinates for the fluid and, if necessary, for the structure.

Other authors [11-17] have proposed non standard finite element formulations for acoustic fluids in the analysis of fluid-structure interaction problems. These consist in introducing new variables for the fluid, thereby leading to symmetric matrix systems that include the displacement formulation [11-12], the velocity potential formulation [12-13], the mixed displacement potential and pressure formulation [14], and the displacement and vorticity moment formulation [15]. By using these formulations, the normal modes of the structure-cavity system can be computed by solving a symmetric eigenvalue problem. The modal expansion method can then be used to estimate the forced response of the dynamic system in a straightforward manner. The most commonly used formulation is the symmetric pressure-displacement potential (u,p,φ) formulation [16-17]. However, these formulations are not implemented in all commercial FE software applications.

In this paper, the fluid-structure problem is solved by using the Patch Transfer Function approach [18]. This approach is based on substructuring surfaces divided into elementary areas called patches and it consists in studying each subsystem independently, in order to build a set of transfer functions defined by using mean values on the patches, hence the term Patch Transfer Functions. Then, the PTFs are assembled by using the superposition principle for the linear passive system along with the continuity relations, leading to the fast resolution of the coupled problem. This approach has been successfully applied to solve acoustic problems in the medium frequency range for automotive applications [18] and acoustic transmission problems with double wall panels [19]. This approach is not based on an assumption of weak coupling between subsystems, thus it can be used to solve problems of fluid-structure interaction in heavy fluid. Initial developments [20] based on partitioning at the fluid-structure interface have shown that using a standard mode expansion to build the cavity-PTF leads to poor convergence of the PTF method in heavy fluid (as opposed to light fluid). To overcome this problem, the residual shape concept was introduced in the cavity-PTF calculation. A residual shape corresponds to the response of the cavity excited by a constant normal displacement imposed on a patch at a specific frequency. The number of residual shapes enriching the modal basis is equal to the number of patches. This ensures the convergence of the modal expansion to estimate the PTF. Unfortunately, a major drawback of substructuring at the fluid-structure interface occurs when the frequency range of interest is well below the critical frequency of the structure, which is generally the case in heavy fluid applications. Indeed, Ouisse et al. demonstrated in [18] that a $\lambda/2$ patch mesh criterion for the coupling surface was sufficient to obtain good results. However, for frequencies well below

the critical frequency, the flexural wavelength in the structure is much smaller than the acoustic wavelength in the fluid. Consequently, the number of patches that must be considered for substructuring at the structure-cavity interface is much greater than that used when substructuring is performed in the fluid medium. However, the position of the coupling surface that partitions the global system into two (or more) subsystems can be defined in different ways. Thus it appears possible to identify an optimal position of the coupling surface to minimize the number of patches. This position should not be defined too far from the structure, in order to limit the size of the corresponding subsystem, while it should not be too close, in order to use a patch mesh criterion based on the acoustic wavelength and not on the flexural wavelength. This paper addresses this specific point.

After having recalled the theoretical background of the PTF method proposed, the definition of an optimal position of the coupling surface is discussed in section 3. This discussion is based on well-known phenomena related to the acoustic radiation of structures below their critical frequencies. A basic analytical model is used to define a criterion for estimating the optimal position of the coupling surface. This criterion ensures that the pressure distribution varies spatially according to the acoustical wavelength on the coupling surface. Beyond this distance, the patch size criterion is assumed as based on the acoustic wavelength. This methodology is validated on an academic test case composed of a rectangular plate coupled with a parallelepiped cavity. Comparisons between a reference result and the PTF results for different substructures show that the distance criterion is well adapted and that a patch mesh criterion based on the half acoustic wavelength can be used to obtain good results. However, this methodology implies the definition of a subsystem composed of the structure and the surrounding fluid. Computing the PTFs of such a subsystem is not an easy task, since the FE model associated with this subsystem is non-symmetric, thereby hindering the use of a standard eigenvalue solver; moreover, direct resolution is time consuming. To offset this difficulty, a non standard modal expansion based on the symmetric formulation proposed in the literature [21] is presented in section 4 to facilitate calculating the PTFs of this subsystem. For the damped problem, symmetrization leads to a complex mass matrix and requires the definition of new modal damping parameters. This formulation also allows computing the residual shapes used to enrich the modal basis exactly as in [20]. This approach is implemented in the FE commercial software MSC/NASTRAN by using DMAP instructions. Comparisons of a direct FE resolution with PTF results by using this modal method on the academic test case highlight its accuracy and efficiency. Finally, the present approach is applied to an industrial case. It consists in calculating the acoustic transmission through the

bulkheads of the ballast compartments of a submarine. To do this, the problem is divided into 5 subsystems. The results obtained show the efficiency of the PTF method in terms of computation time compared to direct FE resolution.

2 Principle of PTF approach

FIGURE 1

Let us consider the internal vibro-acoustic problem presented in Fig 1. The vibrating structure of volume Ω_s is coupled with a rigid-wall acoustic cavity of volume Ω. S_u is the fluid-structure coupling interface and S_r is the rigid wall surface. The structure is assumed to be elastic and excited by a harmonic point force $Fe^{j\omega t}$ where F is the amplitude of the force, ω the angular frequency, and t time. Here, we are interested in the stationary response of the system. In the following, time dependence will be omitted in the notation although it is always considered. The goal of this section is to calculate the responses at point M in the cavity and at point M' of the structure by using the PTF approach.

Basically, the PTF method [18] consists in partitioning the global system into two subsystems, by partitioning volume Ω with a coupling surface S_c, as shown in Fig. 1. The elastic structure coupled with a subcavity of volume Ω_1 is the first subsystem while the other subcavity of volume Ω_2 is the second subsystem ($\Omega = \Omega_1 \cup \Omega_2$). The coupling surface S_c is then divided into N elementary surfaces $\partial S_i, i \in [1, n]$, called patches.

For the sake of clarity, it can be considered that there are only two subsystems in this presentation, but the PTF approach can be easily extended to an arbitrary number of subsystems.

To define the Patch Transfer Functions (PTF), each subsystem is considered independently. For subsystem α (α=[1,2]), a constant normal volume velocity $\overline{q}_i^{\alpha}$ is prescribed on patch i of surface ∂S_i, whereas a null normal velocity is prescribed on the other patches. Thus the PTF of subsystem α is defined by:

- the Patch Transfer Functions between excited patch *i* and receiving patch *j*, Z_{ij}^{α}:

$$Z_{ij}^{\alpha} = \frac{\overline{p}_j^{\alpha}}{\overline{q}_i^{\alpha}}, \tag{1}$$

where $\overline{p}_j^{\alpha}$ is the space-averaged pressure on the patch *j* (*i.e.* $\overline{p}_j^{\alpha} = \frac{1}{\partial S_j}\int_{\partial S_j} p_j^{\alpha}(M)dS$), when patch *i* vibrates with the normal volume velocity $\overline{q}_i^{\alpha}$.

In the present definition, one considers the normal volume velocity $\overline{q}_i^{\alpha}$ instead of the normal velocity $\overline{u}_i^{\alpha}$ considered in [17]. The use of normal volume velocity $\overline{q}_i^{\alpha} = \overline{u}_i^{\alpha}\partial S_i$ allows us considering the reciprocity relation, $Z_{ij}^{\alpha} = Z_{ji}^{\alpha}$. It reduces the number of calculations of the PTFs and it leads to symmetric matrices in the following;

- the Patch Transfer Functions between excited patch *i* and point *M* inside subcavity Z_{iM}^{α}:

$$Z_{iM}^{\alpha} = \frac{p_M^{\alpha}}{\overline{q}_i^{\alpha}}, \tag{2}$$

where p_M^{α} is the resulting pressure at point *M* when patch *i* vibrates with the normal volume velocity $\overline{q}_i^{\alpha}$.

In the following, subsystem 1 containing the structure is excited with a mechanical force *F* acting on the structure. In agreement with the PTF approach, the blocked pressure of patch *i* is defined for this subsystem: $\widetilde{p}_i^1$ as the space-averaged pressure on patch *i* due to the mechanical force *F* when a null normal velocity is imposed on all the patches (i.e. null normal velocity on the coupling surface S_c).

It should be noted that the PTF corresponds to acoustic impedance, since it is defined as the ratio of the mean pressure over the mean volume velocity. These quantities can also be called Patch Acoustic Impedance (PAI). This permits making a distinction between the global approach (i.e. PTF approach) and the quantities defined in this approach for each subsystem (i.e. the PAI).

Coupling the subsystems is performed by:

- using the linearity properties of the system to express the patch pressure by the sum of the pressure corresponding to the source with a rigid boundary surface and the pressure radiated by the patch velocities ([18]):

$$p_i^1 = \sum_{j=1}^{N} Z_{ji}^1 q_j^1 + \tilde{p}_i^1, \text{ and, } p_i^2 = \sum_{j=1}^{N} Z_{ji}^2 q_j^2, \ \forall i \in [1,...,N], \tag{3}$$

- writing the continuity conditions on each patch, namely the equality of pressures and the equality of normal velocities at connecting patches:

$$p_i^1 = p_i^2, \text{ and, } q_i^1 + q_i^2 = 0, \ \forall i \in [1,...,N]. \tag{4}$$

The velocity condition takes into account that the normal velocity of the patches of the different subsystems are in opposing directions.

By introducing (3) in (4), a linear system is obtained with the patch volume velocities q_j^2 as unknowns:

$$\sum_{j=1}^{N} \left[\left(Z_{ji}^1 + Z_{ji}^2 \right) q_j^2 \right] = \tilde{p}_i^1, \ \ \forall i \in [1,...,N]. \tag{5}$$

This linear system must be solved is a full system, but its size is small since the number of unknowns is equal to the number of patches. Its inversion leads to the patch volume velocities values q_j^2 when the two subsystems are coupled together. By using the linear property of the system in a post-processing phase, it is possible to calculate:

- the pressure at point *M* in the subcavity of subsystem 1:

$$p_M^1 = \tilde{p}_M^1 - \sum_{i=1}^{N} Z_{iM}^1 q_i^2 \text{ , and,} \tag{6}$$

- the pressure at point *M'* in the subcavity of subsystem 2:

$$p_{M'}^2 = \sum_{i=1}^{N} Z_{iM'}^2 q_i^2 \text{ ,} \tag{7}$$

where Z_{iM}^1 and Z_{iM}^2 are defined by Eq. (2).

These two relations permit estimating the acoustic pressure at any point of the cavity as long as the patch transfer functions between the considered point and the patches (i.e. Eq. (2)) have been calculated previously.

To estimate the normal displacement at a given point of the structure, it is necessary to introduce two new quantities for subsystem 1 beforehand. Firstly, as with Eq. (2), the Patch Transfer Functions are defined between patch *i* and point *M'* on the structure, $Y_{iM'}^1$:

$$Y_{iM'}^1 = \frac{W_{M'}^1}{\bar{q}_i}, \tag{8}$$

where $W_{M'}^1$ is the resulting normal displacement at point *M'* when patch *i* vibrates with a constant normal volume velocity $\bar{q}_i^1$. Secondly, as subsystem 1 containing the structure is

excited by the mechanical force, the blocked displacement at point M', $\tilde{W}^1_{M'}$ is defined as the displacement at point M' due to external force F when a null normal velocity is imposed on all the patches.

With these quantities and the patch volume velocities, q_i^2, it is possible to calculate the normal displacement at point M' of the structure by using the linear property of the system:

$$W^1_{M'} = \tilde{W}^1_{M'} - \sum_{i=1}^{N} Y^1_{iM'} q_i^2 \; ; \tag{9}$$

The PTF approach then allows calculating the response of a global system from the PAI of uncoupled subsystems by inverting a square symmetric matrix whose dimension corresponds to the number of patches. The PAI can be calculated by different methods depending on the subsystem considered (analytical for academic subsystems, FEM, BEM for complex geometries, Rayleigh integral for semi-infinite medium, etc.). These calculations are performed for each subsystem separately. Consequently, parallel computation is possible. When FEM is used, the size of the numerical models of each subsystem is considerably smaller than that of the global model. Moreover, the use of incompatible meshes at the subsystem interface is possible, since the problem of compatibility is solved by patch averaging.

3 Position of the coupling surface

3.1 Discussion and definition of criterion

In this section, the position of coupling surface S_c is studied. This surface defines the interface between two subsystems. Since a weak coupling assumption is not necessary in the PTF formulation, it is therefore possible to use any surface to partition the global system. This statement has been verified in Ref. [18], in which the acoustic behaviour of a parallelepiped cavity was modelled with the PTF method, by using arbitrary coupling surfaces. It was shown that the PTF approach gives accurate results even if the modes of the uncoupled subsystems are dissimilar to the modes of the global system. Furthermore, a parametric study showed that the size of the patches should be less than half the acoustic wavelength at the highest frequency of interest (i.e. patch size criterion $\lambda/2$) [18]. This criterion was confirmed in Ref.

[19] for PTF modelling of the transmission loss of a double panel. In this case, the wavelength that had to be considered in the criterion was the flexural wavelength of the panel.

In this paper, the structure is loaded by a heavy fluid and the frequencies of interest are well below the critical frequency, which is generally high. The flexural wavelength is thus much smaller than the acoustic wavelength. The role played by these two wavelengths in the fluid medium depends on the distance from the structure. Indeed, when the structure is excited in its near-field, the acoustic pressure varies mainly according to flexural wavelength λ_f of the structure. Thus the patch mesh criterion must be based on the structural wavelength, leading to a large number of patches. On the contrary, outside the near field of the structure, the acoustic pressure varies according to acoustic wavelength λ_a. In this situation, a patch mesh criterion based on half the acoustic wavelength can be applied, thus limiting the number of patches.

FIGURE 2 – TABLE 1

To illustrate this statement, examples are presented in the case of a rectangular simply-supported plate excited by a point force *F* and coupled to a parallelepiped water filled cavity, as shown in Fig. 2. The parameters used in the simulations are given in Table 1. Direct FE calculations are performed with MSC/NASTRAN software.

Fig. 3 presents the pressure distribution inside the cavity for two frequencies: 100 Hz and 700 Hz, well below the critical frequency (around 13400 Hz). In this figure, the plate excited is located at the top of the cavity. It should be noted that the spatial variations of the pressure have a smaller wavelength in the near-field of the plate than in the rest of the fluid domain. The bending wavelength is much smaller than the acoustic wavelength for the two frequencies considered in Fig. 3. The acoustic evanescent waves generated by the plate decrease quickly, perpendicularly to the latter. However, the size of the fluid domain influenced by the bending motions of the plate is not independent of frequency. It is thus necessary to evaluate the optimal position of the coupling surface by ensuring that the acoustic pressure varies according to the acoustic wavelength at the interface of the subsystem, and by limiting the size of the “structure--attached cavity” subsystem

FIGURE 3

To define the cavity attached to the structure, we consider a simpler problem, i.e. the acoustic wave propagation generated by the flexural motions of an infinite plate with a natural bending wavelength. The basic phenomenon demonstrated in the appendix is the evanescent nature of wave propagation in the direction perpendicular to the plate. A criterion is then defined by distance $Z_{\lim}$ from the plate when the radiated pressure has decreased by 10 dB compared to the wall pressure. The developments given in appendix lead to the following expression:

$$Z_{\lim} = \frac{\ln(10)}{2\sqrt{k_f{}^2 - k_0{}^2}}, \tag{10}$$

where k_f is the bending wavenumber of the structure and k_0 is the acoustic wavenumber.

This criterion ensures that the acoustic evanescent waves generated by the structure will be negligible compared to the acoustic travelling wave. Then, from a distance to the structure greater than $Z_{\lim}$ for a given frequency ω, it can be assumed that the pressure distribution varies according to the acoustic wavelength. If the coupling surface is located at a distance greater than $Z_{\lim}$, it is then possible to discretize the coupling surface with a patch criterion based on half the acoustic wavelength. However, $Z_{\lim}$ depends on the frequency. For a plate and for frequencies well below the critical frequency $\left(\text{i.e.}\, k_f{}^2 >> k_0{}^2\right)$, the previous expression can be approximated by:

$$Z_{\lim} \approx \frac{A}{\sqrt{\omega}}, \tag{11}$$

where A is a constant.

This indicates that the lower the frequency, the higher $Z_{\lim}$ is. Since it is useful for practical reasons to perform PTF calculations in a wide frequency range without changing the patch mesh definition, it is necessary to evaluate the distance criterion at the lower frequency of interest. However, a compromise can be found to limit the size of the “structure- attached cavity” subsystem and thus keep the advantages of substructuring in the fluid domain. As the patch size is defined from the smallest half acoustic wavelength in the frequency range of interest, the patch size is lower than the half bending wavelength in the low part of the

frequency band. There is therefore no need to define the coupling surface at a distance greater that the limit distances $Z_{\lim}$ calculated in the low frequency of the band. In other words, the coupling surface can be located in the near field of the structure as long as the patch size is lower than the half bending wavelength. The test case described in Fig. 2 and Tab. 1 illustrates the process used to determine the optimal distance. Patch size criteria $\lambda_f/2$, $\lambda_a/2$ and limit distance $Z_{\lim}$ relating to frequency are presented in Fig. 4. The size of the patches is defined by considering the smaller half acoustic wavelengths in the frequency band of interest [1 Hz-1000 Hz] (i.e. the half acoustic wavelength at 1000 Hz). A patch size of about 0.7 m is obtained for the test case. Patch size is thus greater than the half acoustic wavelengths in the entire frequency band. Moreover, as can be seen in Fig. 4, , patch size is lower than the half bending wavelengths for frequencies below 90 Hz. As the size of the patch conforms to a criterion based on the half bending wavelengths for frequencies below 90 Hz, the coupling surface can be located in the near-field of the plate for these frequencies. This means that the coupling surface can be positioned at a distance lower than limit distances $Z_{\lim}$ calculated for frequencies below 90 Hz. For frequencies above 90 Hz, patch size is greater than half the flexural wavelength. Therefore the coupling surface should be located at a distance greater than $Z_{\lim}$ calculated for frequencies above 90 Hz. From the lower part of Fig. 4, it is possible to deduce that the "optimal" distance from the plate is about 0.3 m (i.e. for frequencies below 90 Hz, $Z_{\lim} > 0.3\,\mathrm{m}$, whereas $Z_{\lim} < 0.3\,\mathrm{m}$ for frequencies above 90 Hz).

FIGURE 4

To verify this reasoning, two different substructurings of the test case are considered. In the first case, the coupling surface is defined at 0.05 m, i.e. at a distance less than $Z_{\lim}$ for all the frequencies in the band, while in the second one, the coupling surface is defined at the "optimal" distance from the plate, as discussed above (i.e. 0.3 m).

FIGURES 5-6

The subsystem meshes corresponding to these two substructurings are shown in Figs. 5 and 6. The coupling surface is discretized into 9 patches for both cases (patch size: 0.67m x 0.5m). The computations of the PAI are performed by a direct resolution of the FE problem related to each subsystem (SOL108 in MSC/NASTRAN Software). These PAI are then used in the PTF approach, as described in section 2, to obtain the forced response of the coupled subsystems. A reference result for this test case is obtained by a direct resolution of the FE problem for the global system. Comparisons of the two PTF results with the reference one are proposed in Figs. 7 and 8 in terms of point responses on the plate and in the cavity, respectively. It can be seen the first substructuring gives poor results, except in the low part of the frequency band. This is due to the fact that the patch size has been defined from a criterion based on the half acoustic wavelength, whereas the coupling surface is located in the near field of the plate. On the contrary, the second substructuring gives accurate results for the entire frequency band, although the patch definition is the same as for the first substucturing. This result clearly shows that a patch mesh criterion based on half the acoustic wavelength can be considered as long as the coupling surface is located at the “optimal” distance defined previously. The definition of this “optimal” distance is the cornerstone of the substructuring method proposed, since it must be defined carefully to obtain accurate results without dramatically increasing the size of the structure-cavity subsystem.

FIGURES 7-8

4 Estimation of the PAI of the cavity-structure subsystem by using modal expansion

4.1 Introduction

In the previous section, the PAIs of each subsystem were obtained by directly resolving the linear equation system of the corresponding FE model. These calculations can be time consuming which is why using a modal approach is proposed in this section to accelerate the PAI calculations. Using modal expansion to calculate the PAI of subsystem 2 of the test case is straightforward. For example, the extraction of the cavity modes of the acoustic cavity subsystem can be easily achieved by using the Lanczos method. On the contrary, the matrices

of the standard FE model are not symmetric for the structure-cavity subsystem including a fluid-structure interaction. Consequently, classical methods such as the Lanczos method, which allow extracting eigenvalues and eigenvectors of a generalized eigenvalue problem, cannot be applied directly. Some authors [11-17] have proposed different non standard formulations of the fluid-structure interaction problem by introducing new variables in the fluid domain. In this section, we propose a modal approach to calculate PAIs starting from the non-symmetric matrices of a standard FE model of the fluid-structure interaction problem. The process can be easily implemented in commercial FEM software applications, such as MSC/NASTRAN.

4.2 Formulation

Let us consider a structure-cavity subsystem excited by an external point force F_e applied on the structure. It can be assumed that the surface coupled with another subsystem is divided into N patches. In order to compute the PAI of this subsystem, it is necessary to take into account the N external loads corresponding to the excitation of each patch with a unit normal velocity, independently of the other patches, and the external force, to calculate the blocked pressure of this subsystem. All in all, the force responses of the subsystem must be calculated for an $N+1$ loaded case and for different frequencies contained in the frequency band of interest $\Delta\omega$. In the following, a modal approach is developed to achieve these calculations.

In the approach proposed, the PAI of the structure-cavity subsystem are derived from its FE model. At a given angular frequency ω, the classical (U,P) formulation of this subsystem is written as follows: (see [20,21]) :

$$\begin{bmatrix} K_S & -A \\ 0 & K_F \end{bmatrix} \begin{Bmatrix} U \\ P \end{Bmatrix} - \omega^2 \begin{bmatrix} M_S & 0 \\ A^T & M_F \end{bmatrix} \begin{Bmatrix} U \\ P \end{Bmatrix} = \begin{Bmatrix} F \\ Q \end{Bmatrix} \tag{12}$$

where: - U and P represent the nodal displacements of the structure and the nodal pressure in the cavity, respectively;

- F are the nodal forces applied on the structure, and Q the nodal volume velocities imposed in the cavity;

- M_S and K_S are respectively the mass and stiffness matrices of the structure;

- M_F and K_F are respectively the mass and stiffness matrices of the cavity;

- A is the fluid-structure interaction matrix, and;

- subscript T refers to the transposed matrix.

The damping effect is introduced by considering a complex Young modulus for the structure and a complex celerity in the fluid. K_S and K_F are therefore complex matrices.

As the matrices of Eq. (12) are not symmetric, classical methods cannot be used directly for extracting the normal modes. To bypass this difficulty and symmetrise the problem, we premultiply Eq. (12) by the following matrix ([21]):

$$S = \begin{bmatrix} {K_S}^T {M_S}^{-1} & 0 \\ -A^T {M_S}^{-1} & I \end{bmatrix}. \tag{13}$$

Therefore a symmetric matrix system is obtained:

$$\left[\overline{K} - \omega^2 \overline{M}\right]\overline{X} = \overline{F}, \tag{14}$$

where:

$$\begin{aligned} \overline{X} &= \begin{Bmatrix} U \\ P \end{Bmatrix}, \overline{K} = \begin{bmatrix} {K_S}^T {M_S}^{-1} K_S & -{K_S}^T {M_S}^{-1} A \\ -A^T {M_S}^{-1} K_S & K_F + A^T {M_S}^{-1} A \end{bmatrix}, \\ \overline{M} &= \begin{bmatrix} {K_S}^T & 0 \\ 0 & M_F \end{bmatrix}, \overline{F} = \begin{Bmatrix} {K_S}^T {M_S}^{-1} F \\ -A^T {M_S}^{-1} F + Q \end{Bmatrix}. \end{aligned} \tag{15}$$

The inversion of the mass matrix of the structure is straightforward for an FE model with lumped masses:

$${M_S}^{-1} = \begin{bmatrix} \ddots & & 0 \\ & \dfrac{1}{m_{ii}} & \\ 0 & & \ddots \end{bmatrix}. \tag{16}$$

Unfortunately, the rotational inertia terms of the mass matrix are often omitted. The matrix is thus singular. It is then necessary to condense the rotation dofs of the structure before inverting the resulting mass matrix. The calculations are time consuming, but they only have to be performed once.

As $\overline{M}$ and $\overline{K}$ matrices are symmetric, the generalised eigenvalue problem can be written as:

$$\left[\mathrm{Re}\left\{\overline{K}\right\} - \lambda\, \mathrm{Re}\left\{\overline{M}\right\}\right]\overline{X} = 0. \tag{17}$$

The Θ first eigenvalues λ_n and the associated mass-normalized eigenvectors ϕ_n are computed numerically, by implementing a modal extraction method (e.g. the Lanczos method):

$${\phi_n}^T\, \mathrm{Re}\left\{\overline{M}\right\}\phi_n = 1,\ {\phi_n}^T\, \mathrm{Re}\left\{\overline{K}\right\}\phi_n = \lambda_n,\ n \in [1,2,..,\Theta]. \tag{18}$$

Residual shapes are introduced [20] to improve the convergence of the modal expansion based on these coupled modes. This technique consists in enriching the modal basis with the quasi-static responses due to the different excitations and by re-orthogonalizing the resulting modal basis to keep the advantages of modal expansion. In our case *N+1* load cases are considered, corresponding to the excitations of each patch and the external load. At a specific angular frequency ω_c, the residual shapes φ_i due to *N+1* excitations $\overline{F}_i$ are calculated:

$$\left[\mathrm{Re}\left\{\overline{K}\right\} - \omega_c^{\,2}\,\mathrm{Re}\left\{\overline{M}\right\}\right]\varphi_i = \overline{F}_i\,. \tag{19}$$

A new reduction basis *P* is defined from these residual shapes:

$$P = \left\{\phi_1 \ldots \phi_\theta \middle| \varphi_1 \ldots \varphi_{N+1}\right\} \tag{20}$$

In order to re-orthogonalize these vectors, the change of base $\overline{X} = P\overline{\overline{X}}$. is introduced in Eq (17). The projection in the *P* basis of the resulting equations gives the reduced generalized eigenvalue problem:

$$\left[\overline{\overline{K}} - \lambda\overline{\overline{M}}\right]\overline{\overline{X}} = 0\,, \tag{21}$$

with

$$\overline{\overline{M}} = P^T\,\mathrm{Re}\left\{\overline{M}\right\}P\,,\ \overline{\overline{K}} = P^T\,\mathrm{Re}\left\{\overline{K}\right\}P\,. \tag{22}$$

All eigenvalues λ'_α and associated eigenvectors v_α of the eigenvalue problem (21) can be calculated easily (for example, by using Givens method [22]). Assuming the eigenvectors are mass-normalized and considering the change of coordinates,

$$\chi_\alpha = Pv_\alpha\,, \tag{23}$$

the following orthogonality relations are verified:

$$\chi_\alpha{}^T\overline{M}\chi_\alpha = 1,\ \chi_\alpha{}^T\overline{K}\chi_\alpha = \lambda'_\alpha\,, \tag{24}$$

$$\chi_\beta{}^T\overline{M}\chi_\alpha = 0\,,\chi_\beta{}^T\overline{K}\chi_\alpha = 0 \quad \text{if } \alpha \neq \beta. \tag{25}$$

Now, to estimate the forced response $\overline{X}$ from Eq. (14) due to excitation F_i, an approximate solution can be found in the new basis $P' = \left\{\chi_1 \ldots \chi_{\Theta+N+1}\right\}$

$$\overline{X} = P'\Gamma \tag{26}$$

where Γ is the vector of the modal amplitudes.

To this end, this expression is introduced in Eq. (14) and the projection of the resulting equation in the P' basis is achieved.

As is done classically in the case of weak damping (Basile assumption, [23]), the off-diagonal terms of the imaginary part of modal matrices are neglected:

$$\chi_\alpha{}^T \,\mathrm{Im}(\overline{M})\chi_\beta \approx 0\,,\ \chi_\alpha{}^T \,\mathrm{Im}(\overline{K})\chi_\beta \approx 0\,,\ \text{if } \alpha \neq \beta. \tag{27}$$

Moreover, the modal damping factors, ζ_α and η_α and the generalized force, $F_{i\alpha}$ are defined as follows:

$$\zeta_\alpha = \chi_\alpha{}^T \,\mathrm{Im}(\overline{M})\chi_\alpha\,,\ \ \eta_\alpha = \chi_\alpha{}^T \,\mathrm{Im}(\overline{K})\chi_\alpha\,,\ \text{and,} \tag{28}$$

$$F_{i\alpha} = \overline{F}_i \chi_\alpha\,. \tag{29}$$

By doing the above, the result of the projection in the P' basis gives the modal amplitudes Γ_α under the general form:

$$\Gamma_\alpha = \frac{F_{i\alpha}}{-(1+j\zeta_\alpha)\omega^2 + (1+j\eta_\alpha)\omega_\alpha^2}, \forall \alpha \in [1, \Theta + N + 1], \tag{30}$$

where ω_α is the natural angular frequency given by $\omega_\alpha = \sqrt{\lambda'_\alpha}$

Using (26) and (30), the response of the structure-cavity subsystem is computed from the coupled modes $(\omega_\alpha, \chi_\alpha)$. It can be seen that the symmetrization procedure of the standard formulation of the fluid-structure problem leads to complex mass and stiffness matrices. As a result, two damping factors ζ_α and η_α must be introduced in the modal method. Their values depend on the damping factors associated with the structure and the cavity, and on the mode shapes.

To estimate the PAI between patch *i* and patch *j*, a unit normal volume velocity must be imposed on the surface of patch *i*, ∂S_i. In the finite element formulation, it is written by:

$$F = 0, \text{for all nodes}\,,\ \text{and,}\ Q = \begin{cases} -j\dfrac{\omega}{n_i}\ \text{, for the } n_i \text{ nodes } \in \partial S_i, \\ 0 \qquad\quad \text{, otherwise.} \end{cases} \tag{31}$$

The PAI Z_{ij} is then estimated by the expression:

$$Z_{ij} = \sum_{i=1}^{\Theta+N+1} \frac{F_{i\alpha}\chi_{j\alpha}}{-(1+j\zeta_\alpha)\omega^2 + (1+j\eta_\alpha)\omega_\alpha}, \tag{32}$$

where $\chi_{j\alpha}$ is the mean value of χ_α on patch *j*.

A DMAP procedure [24] was run on MSC/NASTRAN to perform the calculations of the coupled modes and the residual shapes described in this section. The modal information was then used in a MATLAB program to calculate the PAIs from Eq. (32).

4.2 Numerical validation

In this section a numerical validation of the PAI calculations from the modal approach described previously is proposed. To do this, the test case presented in Fig 2 and the second PTF substructuring (see Fig. 6) are considered.

The coupled modes of the "structure-attached cavity" subsystem were estimated from the process described previously. The original modal basis contains the normal modes with their natural frequencies below 1500 Hz (i.e. 100 normal modes). Moreover, this modal basis is enriched by 10 residual shapes corresponding to the 9 patch excitations and the external load acting on the plate. The specific angular frequency ω_c has been set to 314 rad/s (100 Hz). The results are not sensitive to this parameter as long as this specific frequency is not equal to a natural frequency of a coupled mode and its value remains below the frequency of the last coupled normal mode retained in the modal expansion (see discussion in [20]). The values of the modal damping factors ζ_α and η_α are presented in Fig. 9.

FIGURE 9

These values depend on the cavity damping value, namely 0.001, and the plate damping value, namely 0.01. For the low modal order, the values of ζ_α are close to the value of the plate damping factor. This can be explained by the fact that the cavity has a non-resonant behaviour for the low frequencies considered and that the coupled modes are dominated by the plate modes. For a higher modal order, the coupled modes correspond to strong coupling between plate modes and cavity modes. Thus, the values of ζ_α and η_α vary between the plate and the cavity damping values. For the residual shapes, the values of η_α are generally close to the plate damping value and are greater than that of ζ_α. However, since the natural frequencies of the residual shape modes are located between 2259 Hz and 5225 Hz, their

responses for frequencies below 750 Hz are non resonant and do not depend on their damping values.

FIGURES 10-12

In Fig. 10 the results obtained for the blocked pressure by three methods are presented. The first method is the reference one and consists in a direct resolution of the FE problem; the second is the present modal method without residual shapes, and the last is the present modal method including the residual shapes. Similar comparisons are proposed in Fig. 11 and Fig. 12 for the input PAI of patch 1 and for the transfer PAI between patch 1 and patch 3, respectively.

In Figs. 10 and 12, it can be seen that the modal approach without residual shape modes allows converging in the resonant domains of the spectrum, whereas several discrepancies can be observed in the non-resonant domains. The natural frequencies of the coupled modes are therefore correctly estimated by the present approach, but these coupled modes do not allow representing the non-resonant behaviour of the cavity-structure system. Moreover, for the input PAI (see Fig. 11), the discrepancies between the modal results and the reference result appear at all frequencies above 100 Hz. This is due to the poor convergence of modal expansion for an acoustic cavity, as illustrated in Ref. [20]. Consequently, a large number of non-resonant modes are required to ensure the convergence of the PAI calculation. However, using residual shape modes considerably improves the convergence of the modal expansion. This can be observed in Figs. 10-12 where the curves of the reference results and those of the modal expansion with residual shapes match very well.

FIGURES 13-14

These PAIs calculated from the modal method are then used in the PTF approach to calculate the global response of the test case. The structural accelerations and the acoustic pressures obtained from the PTF approach are compared with the reference results in Figs. 13 and 14, respectively. It can be seen that the poor convergence of the PAIs calculated without the residual shape modes leads to significant errors in the PTF calculation of the acoustic pressure

inside the cavity. On the contrary, using residual shape modes provides good results. Tab. 2 shows the MSC/NASTRAN computing times required for the different calculations performed on the test case. They indicate that a significant decrease in computing-time is obtained with the modal method proposed in comparison to a direct FE calculation.

In conclusion, the modal approach described in this section permits calculating the PAI of each subsystem accurately and efficiently compared to a direct FE calculation.

TABLE 2

5 Submarine application: sound transmission through ballast compartments

A numerical application on a naval industrial case is proposed to illustrate the advantages of the approach presented. It concerns the assessment of the self-noise on the bow sonar of a submarine. Self-noise is the noise generated by the submarine on its acoustic arrays. In some situations, this noise can disturb the reception of acoustic sensors and limit their detection performance. One of the sources of this self noise could be the radiation of the end of the pressure hull excited by internal mechanical sources. The acoustic energy could then propagate from the end of the pressure hull to the bow Sonar cavity through the ballast compartments. The application proposed in this section is a simplified problem consisting in modelling sound transmission through two ballast compartments located at the front of a submarine.

5.1 Description of the problem

FIGURE 15

Let us consider the ballast compartments described in Fig. 15. The structure is composed of three simply supported elastic bulkheads coupled by two rigid-wall water-filled cavities. The

thick bulkhead on the right-side of Fig. 15, which represents the end of the pressure hull, is excited by a point mechanical force in the frequency band [1Hz-1000Hz]. The aim is to assess the acceleration levels on non excited bulkheads due to the energy transmission through the cavities.

The geometry of the system corresponds to a quarter part of a truncated cone 17.3m long with a diameter varying from 4m to 5m. The bulkheads are portions of spheres with radii ranging from 20m to 29.3m, as shown in Fig. 15. They are made of steel (ρ=7800 kg/m^3, E=2.1x10^{11} Pa, ν=0.3, η=0.01), with a constant thickness of 50mm for the excited bulkhead, and 22mm for the others. The two cavities are filled with water (ρ=1000 kg/m^3, c=1500m/s, η=0.001). The excitation is a unit point force acting on the thick bulkhead along the x-axis at point (17.76 m, 2.77 m, 2.77 m). An FE model of the whole system has been built on the basis of 6 elements per wavelength at 1000 Hz. It is composed of 106522 nodes, 5953 CQUAD4 elements and 520422 CTETRA elements.

5.2 Application of the PTF approach

The substructuring introduced in section 3 is applied to the present application to define the PTF subsystems. As the whole system is made up of three bulkheads coupled by two cavities, each bulkhead can be integrated in a different subsystem with its surrounding fluid. Two bulkheads are then loaded by the fluid on one side whereas the last one is loaded on both sides (see Fig. 15).

FIGURE 16

Furthermore, the coupling surfaces are located at the optimal distance from the bulkheads, as discussed in section 3.1. To define this optimal distance, the patch size criterion and Z_{lim} criteria for the equivalent plates are plotted in Fig. 16. A patch dimension of 0.7m is lower than the half acoustic wavelength at 1000 Hz. A criterion of the half bending wavelength of the 50mm-thick plate (resp. 22mm-thick plate) is then respected for frequencies below 250 Hz (resp. 100 Hz), which allows setting the optimal distance to 0.3 m. For practical reasons, a plane geometry for the coupling surfaces is chosen. A minimum of 0.3 m is then imposed between the 4 coupling surfaces and the bulkheads, as shown in Fig. 17. The coupling

surfaces are divided into 151 patches according to a patch mesh criterion based on 2 patches per acoustic wavelength. The FE models of the 5 subsystems are presented in Fig. 18. Finally, it is important to note the practical interest of such substructuring, since the number of dofs of these models is well below the number of dofs of the whole system.

FIGURES 17,18

The modal method, developed in section 4 is used to calculate the PAIs of structure-cavity subsystems 1, 3 and 5. For cavity subsystems 2 and 4, the classical modal approach including residual shapes [20] is used to solve the acoustic problem. Normal modes with natural frequencies below 1500 Hz are taken into account in these modal expansions. The calculations are performed with MSC/NASTRAN software. The computing times and the number of normal modes for each subsystem are given in Tab. 3.

TABLE 3

An identification number from 1 to 151 is attributed to each patch. This number is used to create a PAI matrix for each subsystem. The PAI matrix of subsystem α, $\mathbf{Z}^{\alpha}$ $(\alpha \in [1,5])$ is defined such that the coefficient of row *i* and column *j* is the PAI of subsystem α between the patch of identification number *i* and the patch of identification number *j*. If one or two of the patches considered do not belong to the surface coupling of subsystem α, the coefficient is zero. The dimensions of matrix $\mathbf{Z}^{\alpha}$ are therefore 151×151. Likewise, the blocked pressure vector $\tilde{\mathbf{p}}$ is defined in which the coefficient of row *i* corresponds to the blocked pressure of a patch with identification number *i*.

Then, the PTF methodology described in section 2 is applied for the 5 subsystems. Initially, the pressure on each patch of the 5 subsystems is written by using the superposition principle for linear passive systems; secondly, the continuity conditions of pressure and velocity are written for each patch linked to two subsystems. The patch velocities of subsystem 2 and subsystem 3 are kept unknown. The patch velocities of the other subsystems can be deduced

directly from the previous patch velocities by using the velocity continuity conditions. Then, the coupling volume velocity vector q is defined in which the coefficient of row *i* corresponds to the patch volume velocity of subsystem 2 or subsystem 4 for the patch with identification number *i*.

This methodology is used to obtain the following matrix system:

$$\left[\mathrm{Z}^1 + \mathrm{Z}^2 + \mathrm{Z}^3 + \mathrm{Z}^4 + \mathrm{Z}^5\right]\mathrm{q} = \tilde{\mathrm{p}}, \tag{33}$$

where $\mathbf{Z}^{\alpha}$ is the PAI matrix of subsystem α, $\tilde{\mathbf{p}}$ is the blocked pressure vector, and q is the coupling velocity vector.

By solving Eq. (33), the coupling velocity vector q is obtained. The response of the global system at the receiving points is then easily calculated in a post-processing step, by using the PAIs between the patches and the receiving points.

Even for this case composed of 5 subsystems, the size of the resulting equation system (see Eq. (33)) remains small thanks to a partition performed outside the acoustic near-field of the structures. As a result, this system is solved very quickly. In the present approach, the computation efforts are related to the extraction of the normal modes of each subsystem, which is significantly less time-consuming than for the whole system.

5.3 Comparison with a reference calculation

In this section, the results obtained with the PTF approach are compared to that obtained from a direct FE calculation of the whole vibro-acoustic system considered as a reference. Despite the fact that direct FE calculation gives reliable results, it is very time-consuming when compared to a PTF calculation, since a direct FE calculation lasts 73976 seconds (~ 20.5 hours) versus 13072 seconds (~ 3.6 hours) for a PTF calculation. Comparisons between the reference results and the PTF results are proposed in Figs. 18-21 for the three receiving points defined in Tab. 4.

TABLE 4 - FIGURE 19

In Fig. 19, a comparison of the acceleration level on the excited bulkhead given by three calculations is proposed. The first calculation is the FE calculation that considers subsystem 1 alone with homogeneous Neumann boundary conditions at the interface with subsystem 2. This result corresponds to the blocked acceleration $\tilde{\gamma}^1_{M'}$ (i.e. $\tilde{\gamma}^1_{M'} = -\omega^2 \tilde{W}^1_{M'}$) used in the PTF

approach (see section 2). The second calculation corresponds to the PTF approach including the coupling with the other subsystems, while the last is the direct FE resolution. For the sake of clarity, the results are presented in the frequency band [1Hz -150Hz]. Large differences between the FE results obtained on uncoupled subsystem 1 and that obtained for the whole system can be observed. This indicates that the surrounding fluid considered in subsystem 1 is insufficient to represent the fluid loading of the excited bulkhead. If these calculations were performed on a case with light fluid (e.g., water replaced by air), the differences between the 2 calculations would be negligible. Finally, the good agreement between the PTF and the reference results illustrated in Fig. 19 shows that the PTF approach gives a good description of the fluid loading on the excited bulkhead and the coupling with the other subsystems.

FIGURES 20-22

The comparisons of the whole frequency band presented in Figs. 20-22 give full satisfaction wherever the point of reception is placed. Small shifts of the resonant and anti-resonant peaks can be observed in the upper part of the frequency band. These shifts are not crucial for the analysis of vibro-acoustic behaviour due to the high modal density of the system.

The vibratory levels of the non-excited subsystems are correctly predicted despite the fact that the transmission through the intermediary bulkhead is dominated by the response of non resonant plate modes (i.e. transmission loss is dominated by the mass-law). It should be recalled that these results were obtained by introducing residual shape modes in the modal expansion, as shown previously in section 4.2.

This submarine application clearly shows that the PTF approach is efficient and well adapted to complex systems, since each subsystem is defined by its own FE model and solved independently of the others. Modification of one of the subsystems only leads to a simple update of its PTF as long as the geometry of the structure–cavity interface remains unchanged. Therefore the method is well adapted for re-analysing and optimising the system considered.

Furthermore, the number of patches remains limited due to the substructuring proposed in this paper, and the PTF computing time is reduced once the PAIs have been calculated, which is one of the advantages of the PTF method. Moreover, parallel computation of the PAIs is possible, since these basic quantities are established for uncoupled subsystems. It is also possible to deal with incompatible subsystem meshes. In the application presented here,

compatible meshes have been used to generate a mesh of the whole system and thus formulate the reference calculation. However, the PTF method provides a tool for dealing with incompatible meshes. For subsystems 2 and 4, coarser meshes could be defined on the basis of an element size criterion deduced from the acoustic wavelength divided by 6.
In conclusion, the application of this method to a submarine prow bulkhead structure demonstrates that it is capable of solving complicated problems relating to industrial vibro-acoustic systems and that it is numerically efficient.

6 Conclusion

Improvements of the PTF procedure were proposed in this paper to solve a structure-cavity problem in heavy fluid. It was shown that substructuring outside the near-field of the structure allows reducing the number of patches. An optimal distance between the structures and the coupling surfaces was defined from the analysis of the infinite plate radiation problem. Its validity was then demonstrated on an academic test case. However, such substructuring leads to the definition of a structure-cavity subsystem for which the FE model has non-symmetric matrices. Consequently, standard eigenvalue solvers cannot be used to extract the modes of this subsystem and compute its PAIs. To bypass this difficulty, we used a non-standard modal method based on the direct symmetrization of the standard (U,P) formulation. In the case of the damped problem, symmetrization leads to complex mass and stiffness matrixes. Two modal damping factors were then defined for each mode as a function of the mode shape and the damping factors of the structure and the cavity. Moreover, the residual mode shapes introduced in Ref. [20] were used to improve the convergence of modal series. Comparison with a reference calculation for a complex case highlighted the accuracy and interest of the present approach, which allows reducing computational costs in contrast to the direct resolution of the FE problem.

As the PAIs are calculated for the uncoupled subsystems, independently of the others, the PTF approach can be easily extended to the unbounded fluid domain [25]. In this case, the unbounded fluid domain is considered as a subsystem and the corresponding PAI can be estimated from an integral formulation. An application of this extension to the prediction of Turbulent Boundary layer induced noise inside a submarine SONAR cavity is developed in a doctoral thesis [25].

Acknowledgments

The authors are grateful to the French Ministry of Defence (DGA) for funding this work.

Appendix. Criterion for acoustic evanescent wave attenuation

To define the cavity attached to the structure from a criterion, it is necessary to consider the acoustic wave generated by the flexural motions of an infinite plate. The criterion is then defined by the distance from the plate when the pressure has decreased by 10 dB compared to the parietal pressure. This criterion will ensure that the acoustic evanescent waves generated by the structure will be negligible compared to the acoustic travelling wave.

FIGURE 23

Consequently, the simple two-dimensional problem shown on Fig. 23 is considered. It is composed of an acoustic half-space Ω_∞ with a prescribed normal displacement W imposed on the plane boundary $\partial\Omega_\infty$. The displacement prescribed is defined by the flexural motion of an infinite plate at angular frequency ω. The spatial dependence of this displacement is described by: $W(r)=\tilde{W}e^{-jk_f r}$ where $\tilde{W}$ is the displacement amplitude and k_f the bending wavenumber.

The formulation of this problem is given by [21]:

$$\begin{cases} \Delta p(r,z)+k_0{}^2\,p(r,z)=0, \forall (r,z)\in \Omega_\infty, \\ -\rho_0\omega^2 W(r)=-\dfrac{\partial p}{\partial z}(r,0), \forall r\in \partial\Omega_\infty, \\ R\left(\dfrac{\partial p}{\partial R}+jk_0 p\right)\to 0 \text{ as } R\to\infty, \end{cases} \tag{A.1}$$

where k_0 is the acoustic wavenumber and the last relation is the Sommerfeld radiation condition corresponding to the acoustic free field.

The r-wise variation of the acoustic pressure must follow that of the displacement prescribed [21]. With $p(r,z)=\tilde{p}(z)e^{-jk_f r}$, thus the problem can be rewritten as:

$$\begin{cases} \dfrac{\partial^2 \tilde{p}}{\partial z^2}(z) + \left(k_0{}^2 - k_f{}^2\right)\tilde{p}(z) = 0, \forall z > 0, \\ \dfrac{\partial \tilde{p}}{\partial z}(0) = \rho_0 \omega^2 \tilde{W}, \\ R\left(\dfrac{\partial p}{\partial R} + jk_0 p\right) \to 0 \text{ as } R \to \infty. \end{cases} \tag{A.2}$$

The resolution of the second order differential equation gives:

$$\tilde{p}(z) = \frac{j\rho_0 \omega^2 \tilde{W}}{k_z} e^{jk_z z}, \tag{A.3}$$

where k_z is the solution of the characteristic equation:

$$k_0{}^2 = k_f{}^2 + k_z{}^2. \tag{A.4}$$

Supposing that the bending wavenumber is greater that the acoustic wavenumber ($k_f > k_0$) and considering the Sommerfeld conditions, the single solution for k_z is:

$$k_z = j\sqrt{k_f{}^2 - k_0{}^2}. \tag{A.5}$$

The acoustic pressure in the fluid due to the prescribed displacements is inferred by:

$$p(r,z) = \frac{\rho_0 \omega^2 e^{-\sqrt{k_f{}^2 - k_0{}^2} z}}{\sqrt{k_f{}^2 - k_0{}^2}} W(r). \tag{A.6}$$

This equation expresses the spatial decrease of the acoustic wave radiated by the infinite plate. Therefore the acoustic pressure attenuation from the wall (*z=0*) is defined by:

$$\Delta L_p = 20 \log\left(\frac{p(r,z)}{p(r,0)}\right). \tag{A.7}$$

By introducing Eq. (A.6) in this expression, we obtain:

$$\Delta L_p = -\frac{20}{\ln(10)} \sqrt{k_f{}^2 - k_0{}^2}\, z. \tag{A.8}$$

Therefore a limit distance $Z_{\lim}$ with a criterion of 10 dB attenuation ($\Delta L_p = -10$) can be defined. Lastly, from Eq. (A.8), we deduce:

$$Z_{\lim} = \frac{\ln(10)}{2\sqrt{k_f{}^2 - k_0{}^2}} \,. \tag{A.9}$$

REFERENCES

[1] Caresta, M. and Kessissoglou, N.J., 2011, "Reduction of the sound pressure radiated by a submarine by isolation of the end caps". Journal of Vibration and Acoustics, ASME, **133,** 031008.

[2] Roy, N. and Girard, A., 2005, "Impact of residual modes in structural dynamics". Proceedings of SSMMT, Noordwijk, Netherland.

[3] Roy, N. and Lapi, M., 2008, "Efficient Computation of the Radiated Sound Power of Vibrating Structures using Modal Approach". Proceedings of Acoustics'08, Paris, France.

[4] Balmès, E., 2008, "Theoretical Course Notes: Methods for Vibration Design and Validation". Ecole Centrale Paris, France.

[5] Tournour, M., Atalla, N., Chiello, O. and Sgard, F., 2001, "Validation, performance, convergence and application of free interface component mode synthesis". Computers&Structures, **79**, pp. 1861–1876.

[6] Tournour, M., and Atalla, N., 2000, "Pseudostatic corrections for the forced vibroacoustic response of a structure–cavity system". Journal of the Acoustic Society of America, **107** (5), pp. 2379–86.

[7] Kanarachos, A., and Antoniadis, I., 1988, "Symmetric variational principles and modal methods in fluid-structure interaction problems". Journal of Sound and Vibration, **121** (1) , pp. 77-104.

[8] Ohayon, R., 2004, "Reduced models for fluid-structure interaction problems". International Journal for Numerical Methods in Engineering, **60**, pp. 139-152.

[9] Ohayon, R., 2001, "Reduced symmetric models for modal analysis of internal structural-acoustic and hydroelastic-sloshing systems". Computer Methods in Applied Mechanics and Engineering, **190**, pp. 3009-3019.

[10] Morand, HJ-P, Ohayon, R., 1995, Fluid–structure interaction. New York: Wiley.

[11] Olson, L.G., Bathe, K.J., 1985, "Analysis of fluid–structure interactions – a direct symmetric coupled formulation based on a fluid velocity potential". Computers&Structures, **21**, pp.21–32.

[12] Everstine, G.C., 1981, “A symmetric potential formulation for fluid–structure interactions”. Journal Sound and Vibration, **107**(1), pp.121–9.

[13] Tran, Q.H., Ouisse, M., and Bouhaddi, N., 2010, “A robust component mode synthesis method for stochastic damped vibroacoustics”. Mechanical Systems and Signal Processing, **24,** pp.164-181.

[14] Wang, X., and Bathe, K.J., 1997, “Displacement/Pressure Based Mixed Finite Element Formulations for Acoustic Fluid Structure Interaction Problems”. International Journal for Numerical Methods in Engineering, **40**, pp. 2001–2017.

[15] Bathe, K.J., Nitikipaiboon, C., and Wang, X., 1995, “A mixed displacement-based finite element formulation for acoustic fluid–structure interaction”. Computers&Structures, **6** (2/3), pp. 225–237.

[16] Sigrist, J.F., Garreau, S., 2007, “Dynamic analysis of fluid-structure interaction problems with modal methods using pressure-based fluid finite elements”. Finite Elements in Analysis and Design, **43**, pp. 287-300.

[17] Sigrist, J.F., 2006, “Symmetric and non-symmetric formulations for fluid-structure interaction problems: reference test cases for numerical developments in commercial finite element code”. Proceedings of Pressure Vessel and Piping, Vancouver, Canada.

[18] Ouisse, M., Maxit, L., Cacciolati, C., and Guyader, J.-L., 2005, “Patch Transfer Functions as a Tool to Couple Linear Acoustic Problems”. Journal of Vibration and Acoustics, ASME, **127**, pp. 458–466.

[19] Chazot, J.D., and Guyader, J.-L., 2007, ”Prediction of transmission loss of double panels with a patch-mobility method”. Journal of the Acoustic Society of America, **121** (1), pp. 267– 278.

[20] Aucejo, M., Maxit, L., Totaro, N., and Guyader, J.-L., 2010, “Convergence acceleration using the residual shape technique when solving structure–acoustic coupling with the Patch Transfer Functions method”. Computers&Structures, **88**, pp. 728-736.

[21] Tiliouine, B., and Seghir, A., 1998, “A numerical model for time domain analysis of dams including fluid-structure interaction”. Proceedings of the Fourth International Conference on Computer Structures Technology, Edinburg, UK.

[22] Komzsik, L., 2001, “Numerical methods: user’s guide, MSC NASTRAN 2001”, MSC Software, Santa Ana.

[23] Gmür T., 1997, “Dynamique des structures. Analyse modale numérique”. Presses Polytechniques et Universitaires Romandes, Lausanne.

[24] Reymond, M., 2006, “DMAP Programmer’s Guide, MD NASTRAN 2006 “, MSC Software , Santa Ana.

[25] Aucejo, M., 2010, “Vibro-acoustique des structures immergées sous écoulement turbulent", PhD thesis, INSA Lyon, France.

TABLE CAPTIONS

Table 1. Simulation parameters of the test case.

Table 2. Computing time for the different NASTRAN calculations – PC AMD 64 X2 Dual 3.20 GHz, 2 Go RAM (dof: degree of freedom; rs: residual shapes).

Table 3. Mode number, dofs number and NASTRAN computing time for each subsystem.

Table 4. Position of the excitation point M_0 and the receiving points M_1, M_2, M_3.

FIGURE CAPTIONS

Figure 1. Structure-Cavity problem and PTF substructuring.

Figure 2. Mesh of the plate-cavity test case (9856 nodes, 567 CQUAD4 elements, 7938 CHEXA elements)

Figure 3. Pressure field in the cavity at 100 Hz (upper) and 700 Hz (lower) for the reference test case. Results of direct FEM calculation (MSC/NASTRAN).

Figure 4. Upper part, Patch size criteria $\lambda/2$ for the fluid medium (full line) and for the plate structure (dotted line). Lower part, Z_{lim} parameter defined by Eq. (10). (dash-dotted line symbolised $\lambda/2$=0.7m and Z_{lim}=0.3m for the upper part and the lower part respectively).

Figure 5. Substructuring 1: Subsystem 1: 567 CQUAD4, 567 CHEXA; Subsystem 2: 7371 CHEXA)

Figure 6. Substructuring 2: Subsystem 1: 567 CQUAD4, 2268 CHEXA; Subsystem 2: 5670 CHEXA

Figure 7. Comparison of the acceleration level of the plate at point (1.85, 0.93) for three calculations: dash-dotted line, PTF results with substructuring 1; dash line, PTF results with substructuring 2; solid line, direct FEM results (reference);

Figure 8. Comparison of the pressure level in the cavity at point (1.03,0.93,-0.86) for three calculations: dashed-dotted line, PTF results with substructuring 1; dashed line, PTF results with substructuring 2; solid line, direct FEM results (reference).

Figure 9. Values of damping parameters η and ζ for each modal order: crosses, values for η; circle, values for ζ. Vertical dotted line, splitting between the 100 normal modes and the 10 residual shapes.

Figure 10. Comparison of three methods to estimate the patch blocked pressure of patch 1: dashed-dotted line, modal superposition without residual shapes; dashed line, modal superposition with residual shapes; solid line, direct FEM results (reference);

Figure 11. Comparison of three methods to estimate the input patch acoustic impedance of patch 1: dashed-dotted line, modal superposition without residual shapes; dashed line, modal superposition with residual shapes; solid line, direct FEM results (reference);

Figure 12. Comparison of three methods to estimate the patch acoustic impedance between patch 1 and patch 3: dashed-dotted line, modal superposition without residual shapes; dashed line, modal superposition with residual shapes; solid line, direct FEM results.

Figure 13. Comparison of the acceleration level of the plate at point (1.85, 0.93) for three calculations: dashed-dotted line, PTF results with PAI estimated by modal superposition without residual shapes; dashed line, PTF results with PAI estimated by modal superposition taking the residual shapes into account; solid line, direct FEM results (reference).

Figure 14. Comparison of the pressure level in the cavity at point (1.03,0.93,-0.86) for three calculations: dashed-dotted line, PTF results with PAI estimated by modal superposition without residual shapes; dashed line, PTF results with PAI estimated by modal superposition taking the residual shapes into account; solid line, direct FEM results (reference).

Figure 15. Iso view and top view of the design of the ballast compartments.

Figure 16. Upper part, Patch size criteria $\lambda/2$ for the fluid medium (full line), for the 22 mm thick plate (dash line) and for the 50 mm thick plate (dotted line). Lower part, values of the Z_{lim} parameter for the 22mm thick plate (dash line) and for the 50 mm thick plate (dotted line) (dashed-dotted line symbolised $\lambda/2$=0.7m and Z_{lim}=0.3m for the upper part and the lower part respectively).

Figure 17. Patch definition.

Figure 18. FE model definitions of PTF subsystems.

Figure 19. Comparison of the acceleration level at point M1 for three calculations: dashed-dotted line, FEM results without considering the coupling with the other subsystems (i.e. FEM results of the blocked subsystem); dashed line, PTF results considering the coupling with the other subsystems; solid line, direct FEM results of the whole problem (reference).

Figure 20. Comparison of the acceleration level at point M1 for two calculations: dashed line, PTF results; solid line, direct FEM results (reference).

Figure 21. Comparison of the pressure level at point M2 for two calculations: dashed line, PTF results; solid line, direct FEM results (reference).

Figure 22. Comparison of the acceleration level at point M3 for two calculations: dashed line, PTF results; solid line, direct FEM results (reference).

Figure 23. Semi-infinite 2D fluid medium with imposed displacements at the boundary.

TABLES

Parameters	Values
Plate length	2 m
Plate width	1.5 m
Plate thickness	17 mm
Cavity depth	1 m
Plate density	7800 kg/m^3
Young modulus	2.1×10^{11} Pa
Poisson's ratio	0.3
Plate damping factor	0.01
Water density	1000 kg/m^3
Sound speed in water	1500 m/s
Water damping factor	0.001
Excitation point coordinates	(1.03, 0.93)

Table 1. Simulation parameters of the test case.

Method	Subsystem	Substructuring	Nb of dof / Nb of modes	Computing time
Direct	1 and 2	---	12936 dof	1397 s
Direct	1	1	4828 dof	200 s
Direct	2	1	9200 dof	1688 s
Direct	1	2	6776 dof	542 s
Direct	2	2	7352 dof	755 s
Modal	1	2	100 modes + 10 rs	17 s
Modal	2	2	18 modes + 9 rs	7 s

Table 2. Computing time for the different NASTRAN calculations – PC AMD 64 X2 Dual 3.20 GHz, 2 Go RAM (dof: degree of freedom; rs: residual shapes).

Subsystem	Nb of dof	Nb of modes	Computing time
1	26718	309	5026 s
2	39481	786	617 s
3	26475	545	4814 s
4	31026	637	439 s
5	16003	364	2176 s

Table 3. Mode number, dofs number and NASTRAN computing time for each subsystem.

Point	**Subsys.**	***x (m)***	***y (m)***	***z (m)***
M_0	1	17.76	2.77	2.77
M_1	1	17.61	2.85	1.20
M_2	4	7.34	1.39	2.52
M_3	5	0.17	1.98	1.73

Table 4. Position of the excitation point M_0 and the receiving points M_1, M_2, M_3.

FIGURES

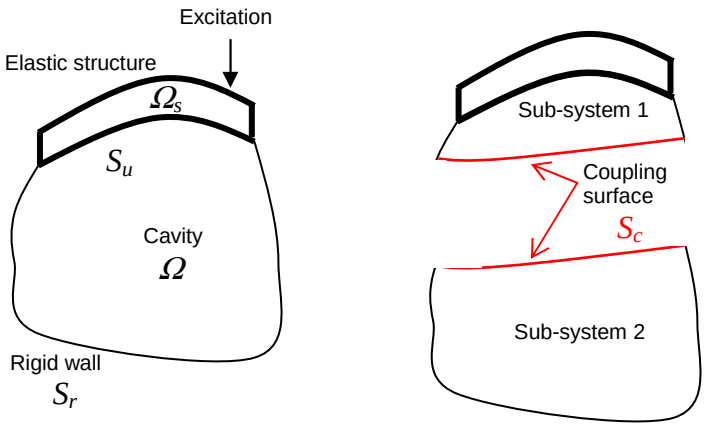

Figure 1. Structure-Cavity problem and PTF substructuring.

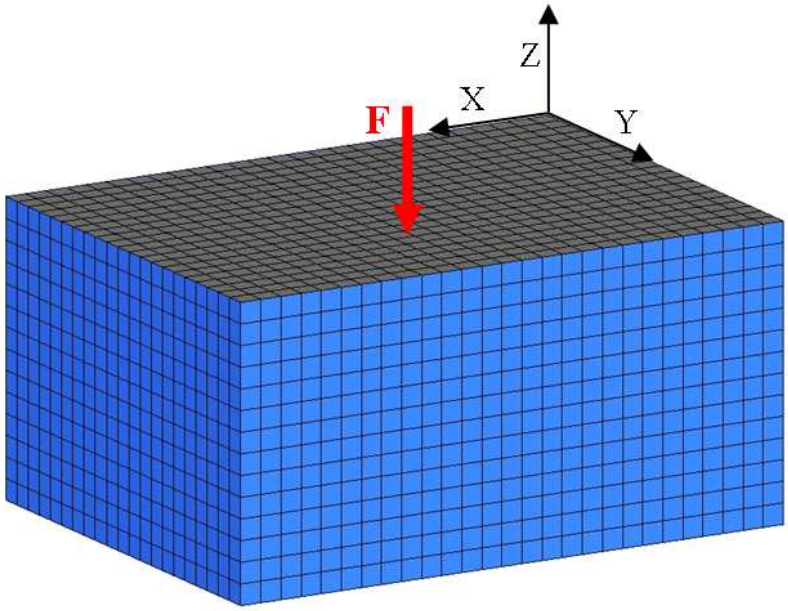

Figure 2. Mesh of the plate-cavity test case (9856 nodes, 567 CQUAD4 elements, 7938 CHEXA elements)

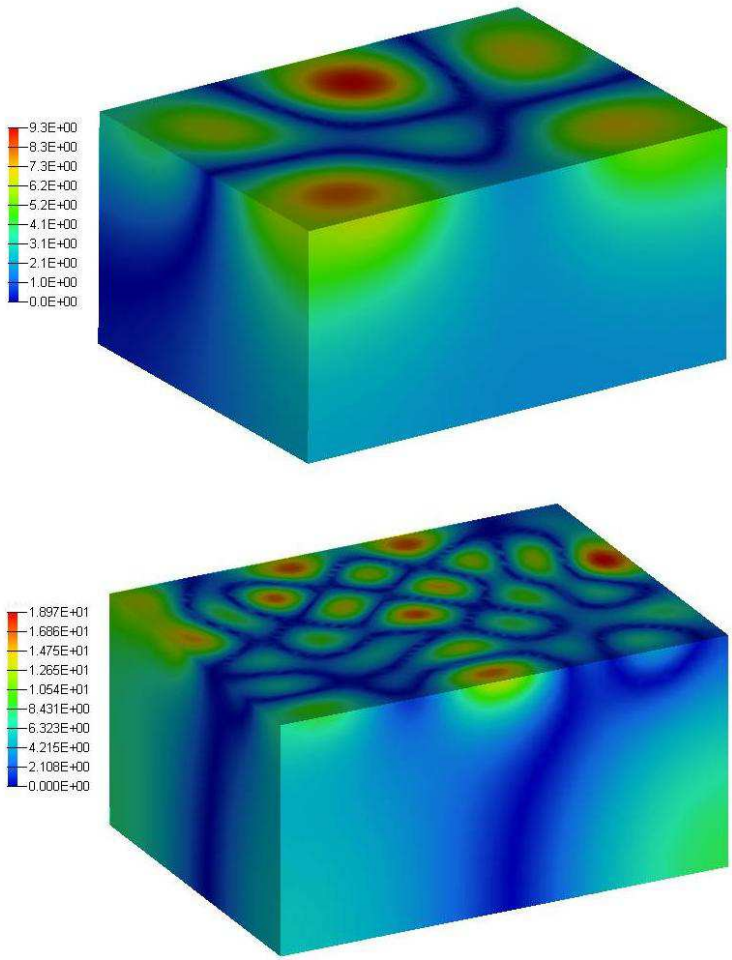

Figure 3. Pressure field in the cavity at 100 Hz (upper) and 700 Hz (lower) for the reference test case. Results of direct FEM calculation (MSC/NASTRAN).

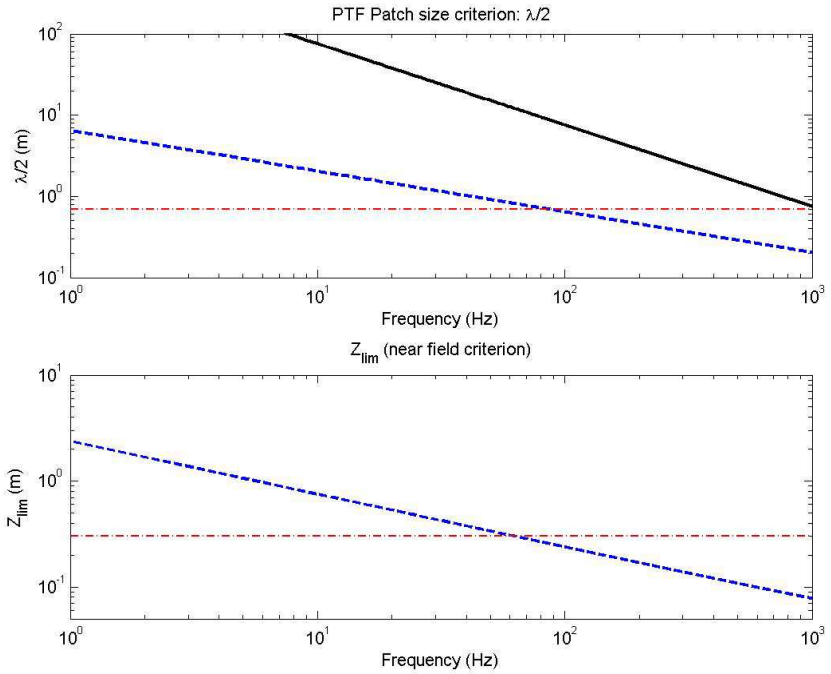

Figure 4. Upper part, Patch size criteria $\lambda/2$ for the fluid medium (full line) and for the plate structure (dotted line). Lower part, Z_{lim} parameter defined by Eq. (10). (dash-dotted line symbolised $\lambda/2$=0.7m and Z_{lim}=0.3m for the upper part and the lower part respectively).

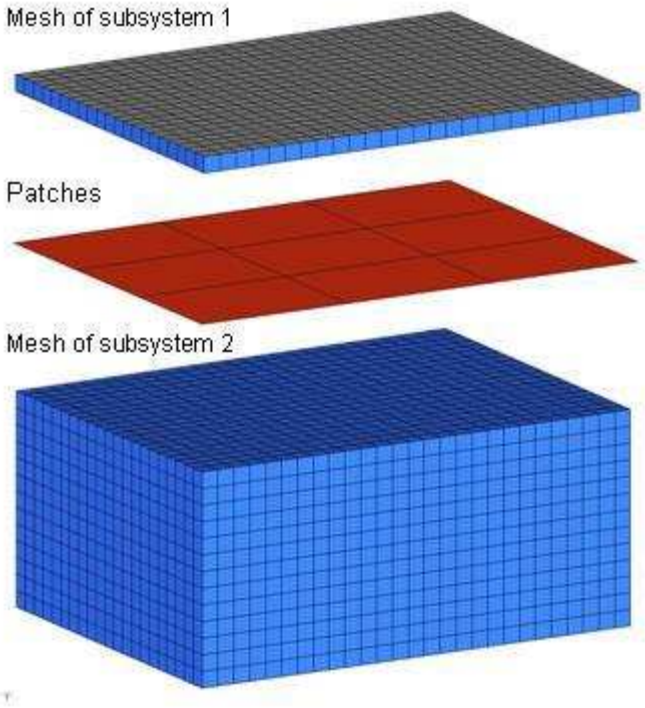

Figure 5. Substructuring 1: Subsystem 1: 567 CQUAD4, 567 CHEXA; Subsystem 2: 7371 CHEXA)

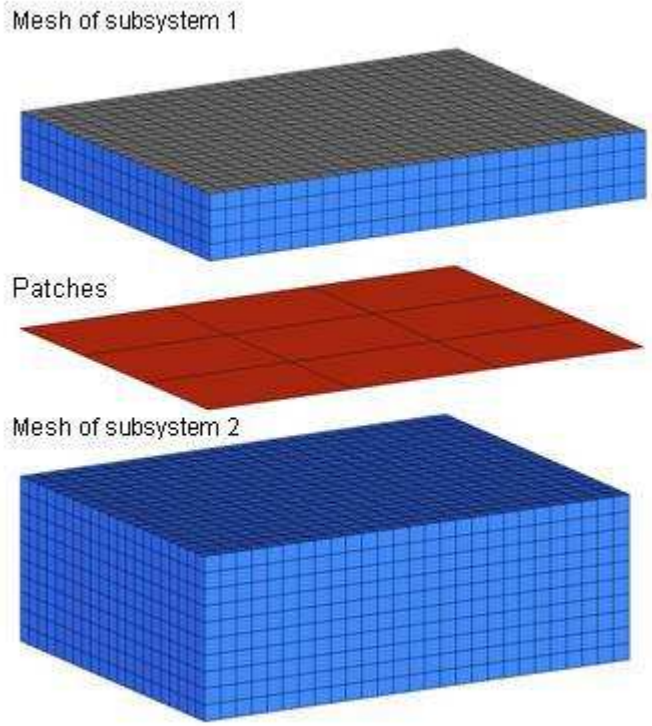

Figure 6. Substructuring 2: Subsystem 1: 567 CQUAD4, 2268 CHEXA; Subsystem 2: 5670 CHEXA

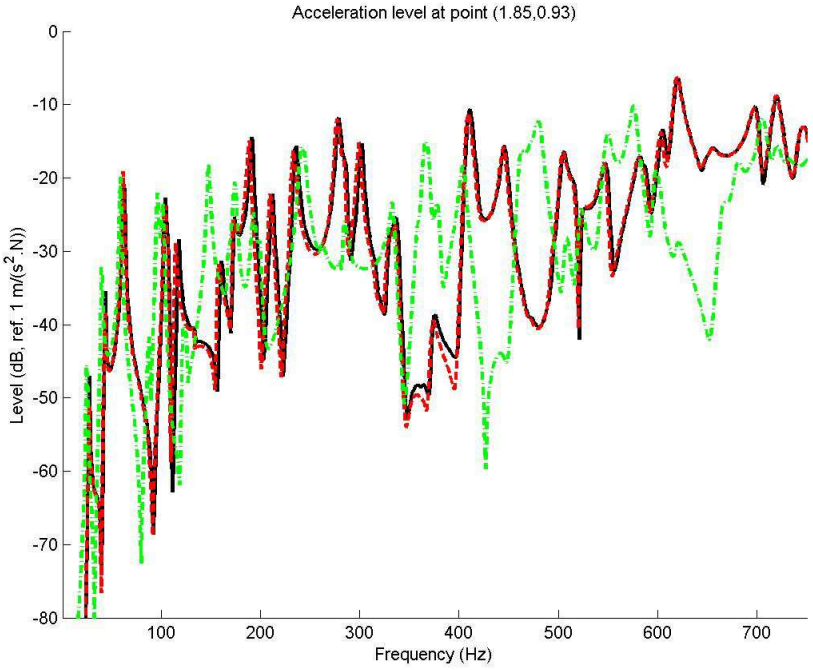

Figure 7. Comparison of the acceleration level of the plate at point (1.85, 0.93) for three calculations: dash-dotted line, PTF results with substructuring 1; dash line, PTF results with substructuring 2; solid line, direct FEM results (reference);

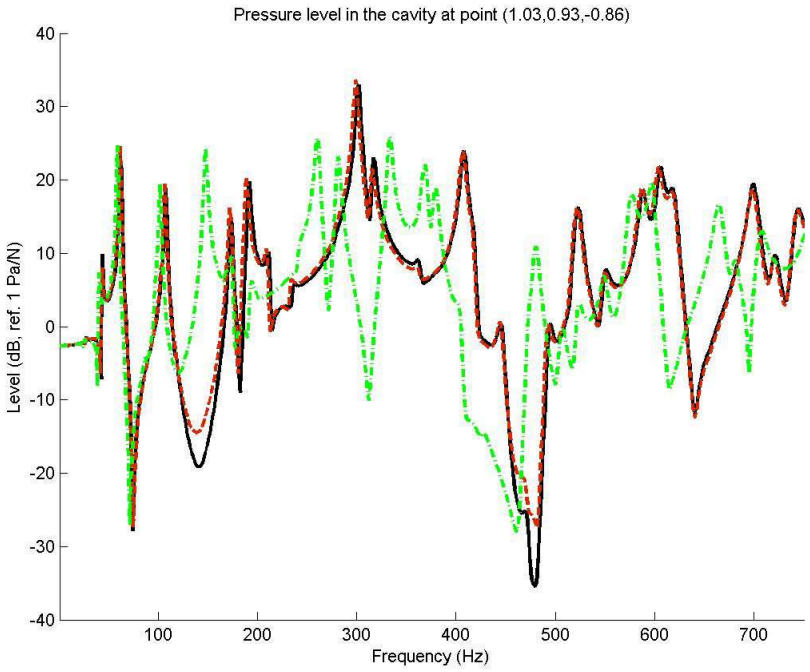

Figure 8. Comparison of the pressure level in the cavity at point (1.03,0.93,-0.86) for three calculations: dashed-dotted line, PTF results with substructuring 1; dashed line, PTF results with substructuring 2; solid line, direct FEM results (reference).

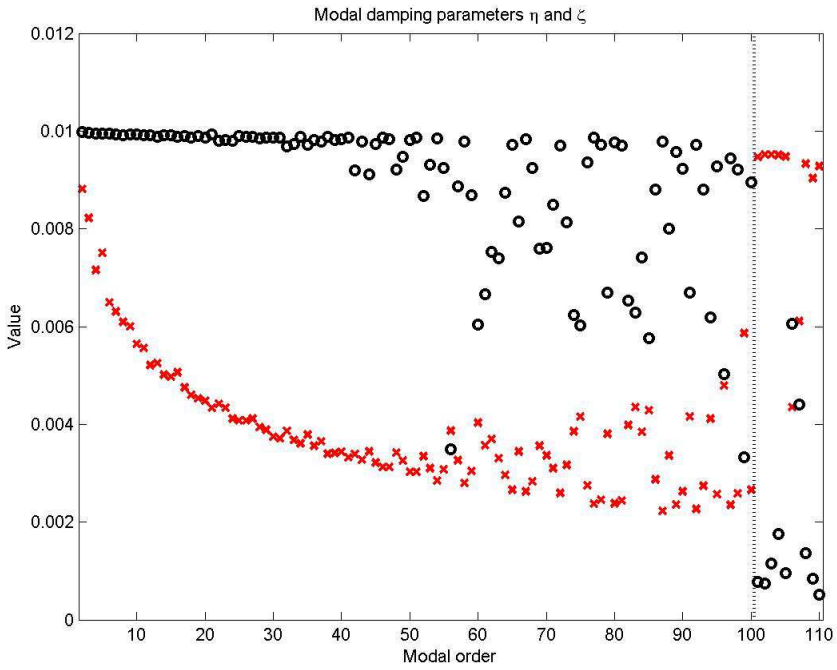

Figure 9. Values of damping parameters η and ζ for each modal order: crosses, values for η; circle, values for ζ. Vertical dotted line, splitting between the 100 normal modes and the 10 residual shapes.

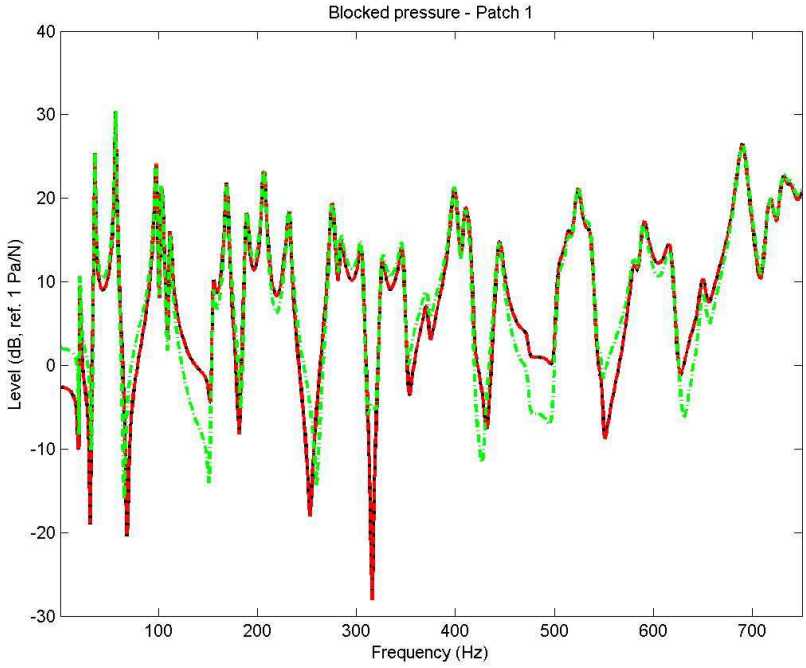

Figure 10. Comparison of three methods to estimate the patch blocked pressure of patch 1: dashed-dotted line, modal superposition without residual shapes; dashed line, modal superposition with residual shapes; solid line, direct FEM results (reference);

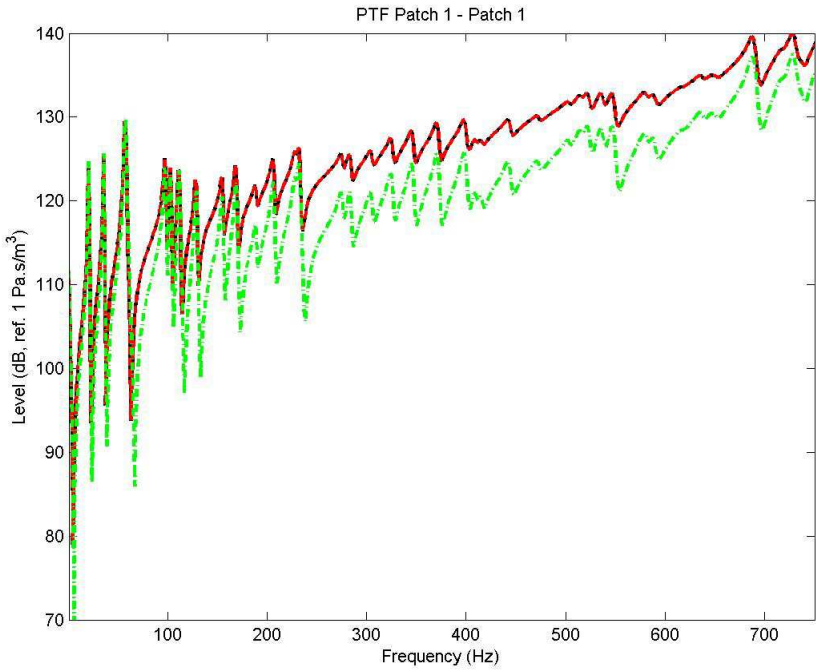

Figure 11. Comparison of three methods to estimate the input patch acoustic impedance of patch 1: dashed-dotted line, modal superposition without residual shapes; dashed line, modal superposition with residual shapes; solid line, direct FEM results (reference);

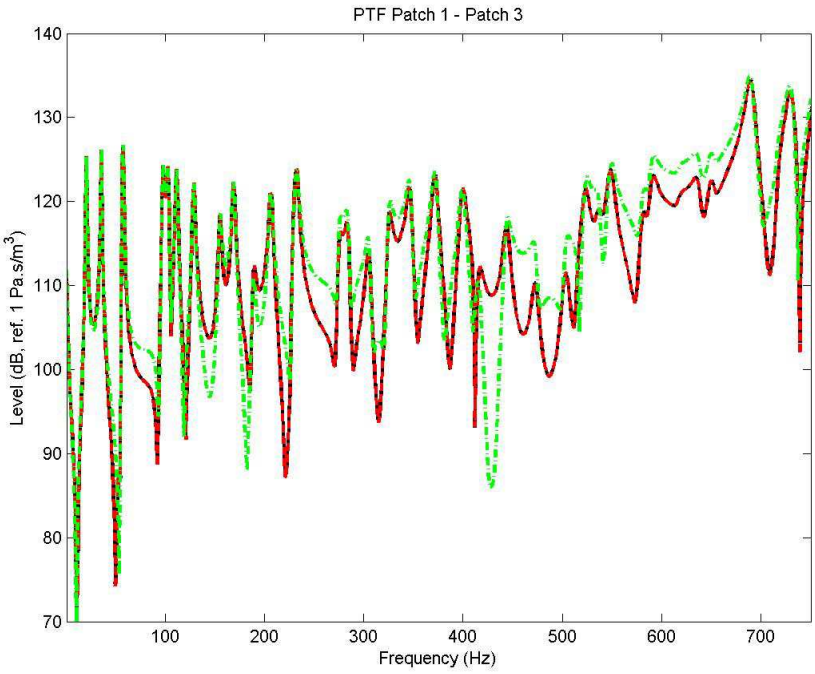

Figure 12. Comparison of three methods to estimate the patch acoustic impedance between patch 1 and patch 3: dashed-dotted line, modal superposition without residual shapes; dashed line, modal superposition with residual shapes; solid line, direct FEM results.

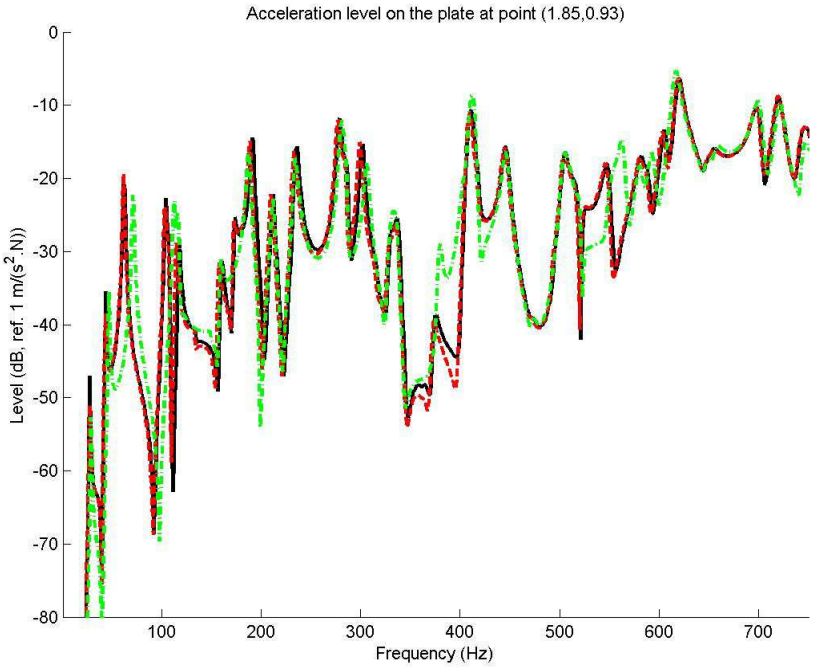

Figure 13. Comparison of the acceleration level of the plate at point (1.85, 0.93) for three calculations: dashed-dotted line, PTF results with PAI estimated by modal superposition without residual shapes; dashed line, PTF results with PAI estimated by modal superposition taking the residual shapes into account; solid line, direct FEM results (reference).

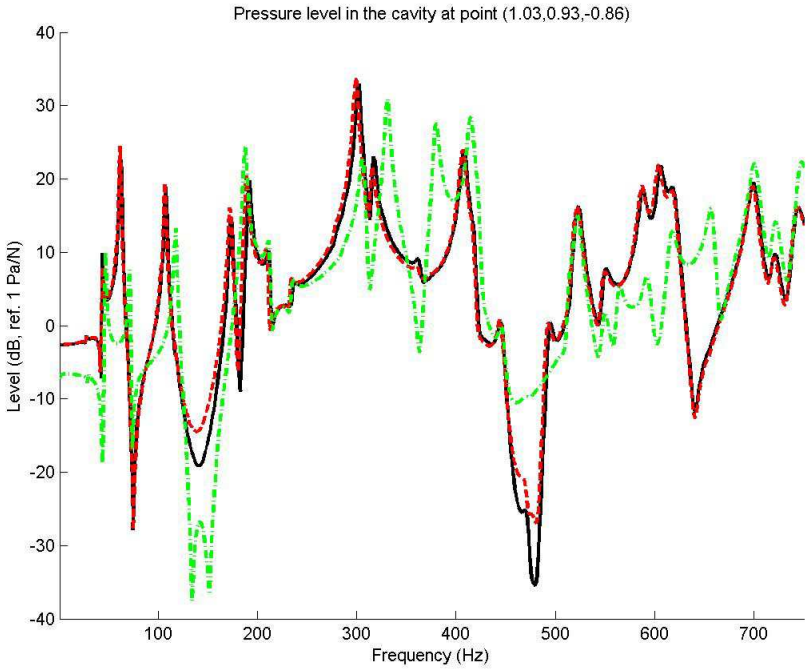

Figure 14. Comparison of the pressure level in the cavity at point (1.03,0.93,-0.86) for three calculations: dashed-dotted line, PTF results with PAI estimated by modal superposition without residual shapes; dashed line, PTF results with PAI estimated by modal superposition taking the residual shapes into account; solid line, direct FEM results (reference).

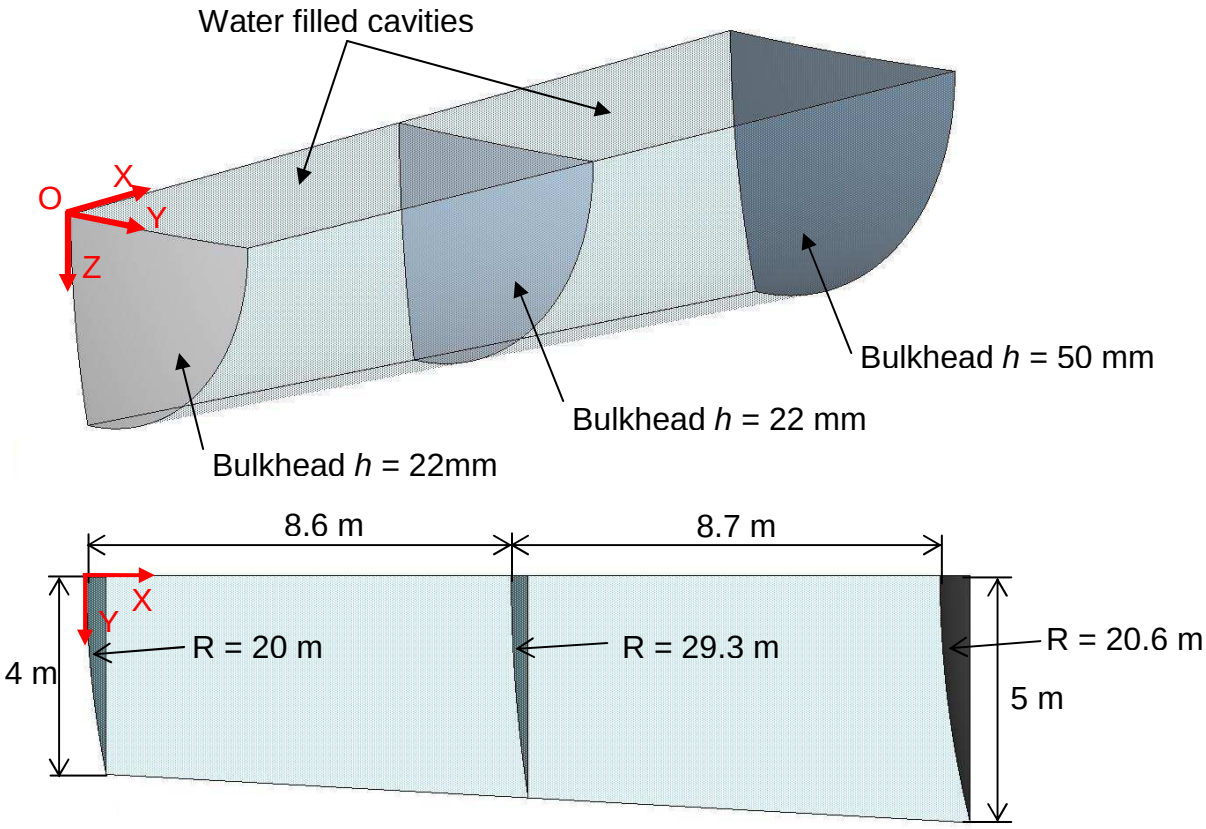

Figure 15. Iso view and top view of the design of the ballast compartments.

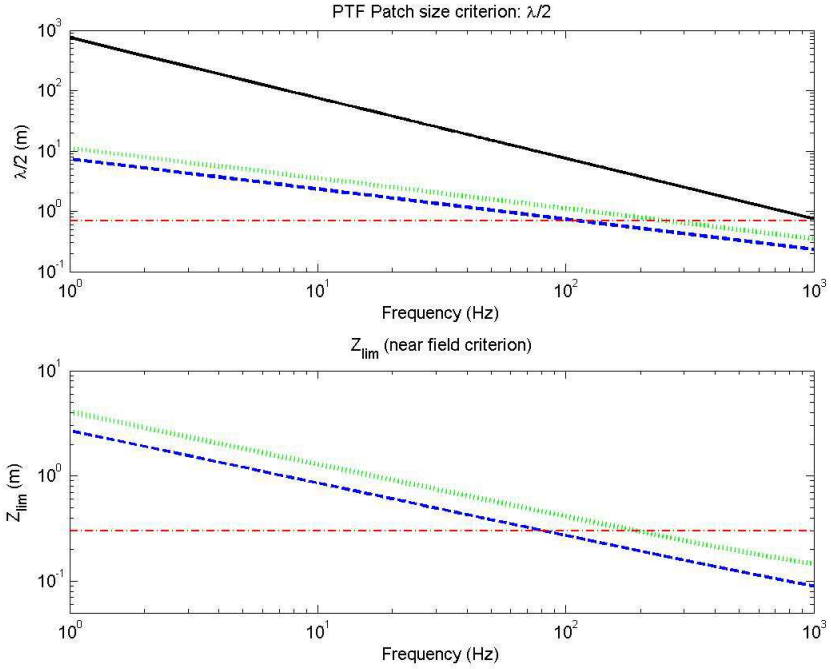

Figure 16. Upper part, Patch size criteria λ/2 for the fluid medium (full line), for the 22 mm thick plate (dash line) and for the 50 mm thick plate (dotted line). Lower part, values of the Z_{lim} parameter for the 22mm thick plate (dash line) and for the 50 mm thick plate (dotted line) (dashed-dotted line symbolised $\lambda/2$=0.7m and Z_{lim}=0.3m for the upper part and the lower part respectively).

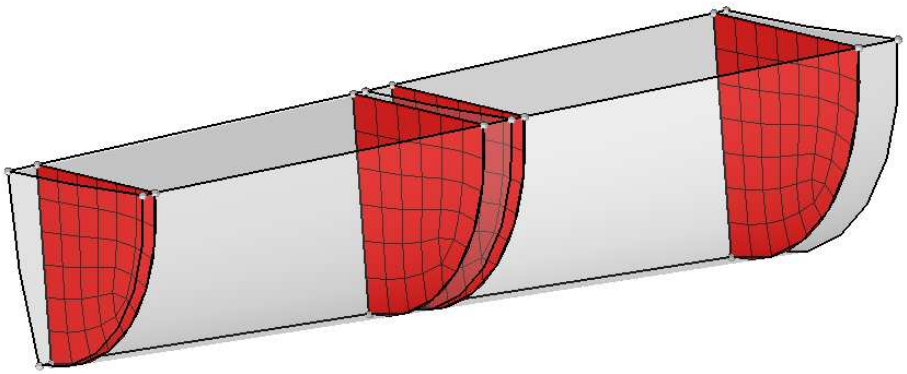

Figure 17. Patch definition.

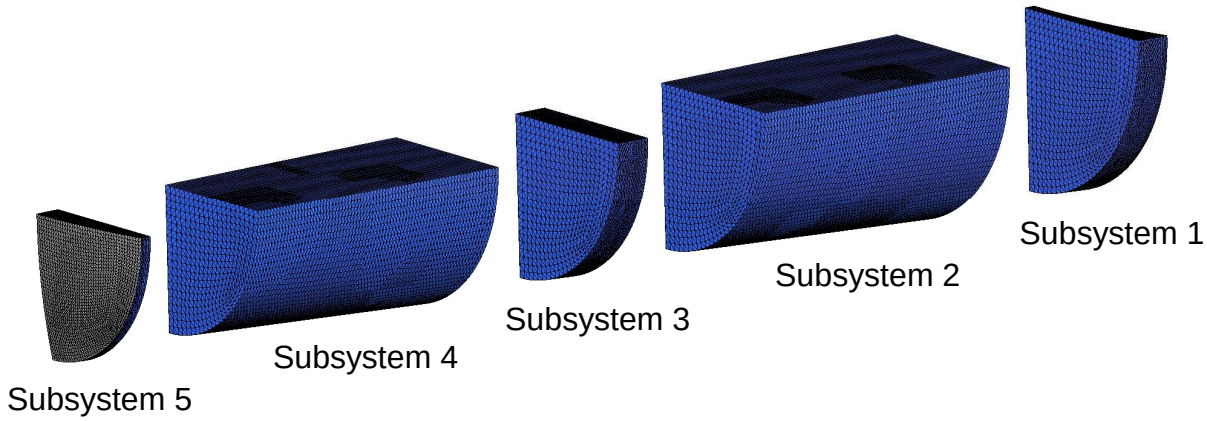

Figure 18. FE model definitions of PTF subsystems.

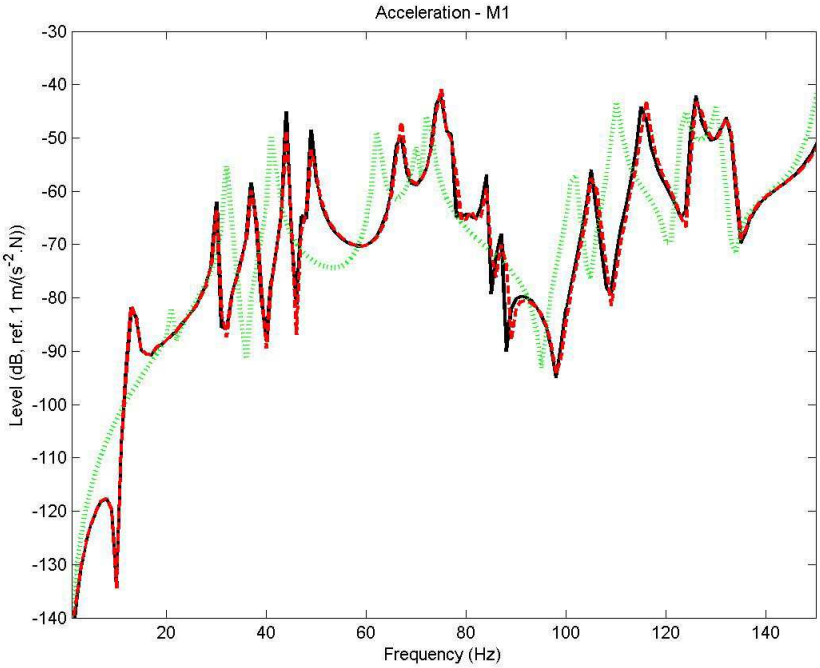

Figure 19. Comparison of the acceleration level at point M1 for three calculations: dashed-dotted line, FEM results without considering the coupling with the other subsystems (i.e. FEM results of the blocked subsystem); dashed line, PTF results considering the coupling with the other subsystems; solid line, direct FEM results of the whole problem (reference).

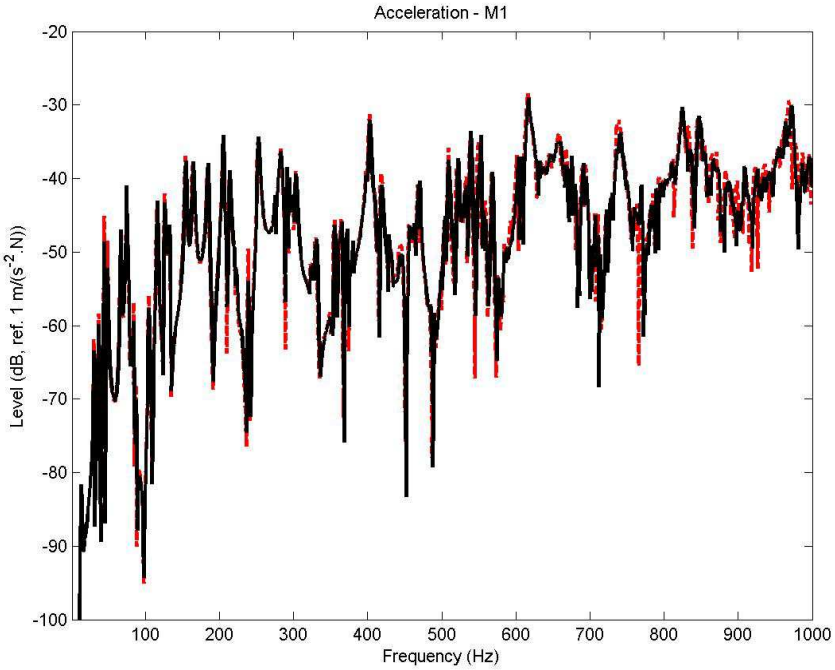

Figure 20. Comparison of the acceleration level at point M1 for two calculations: dashed line, PTF results; solid line, direct FEM results (reference).

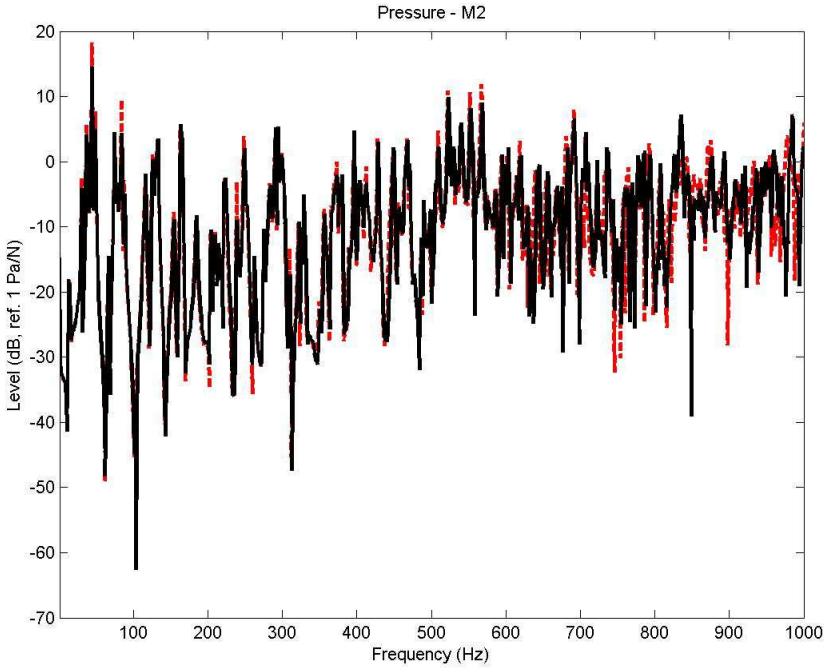

Figure 21. Comparison of the pressure level at point M2 for two calculations: dashed line, PTF results; solid line, direct FEM results (reference).

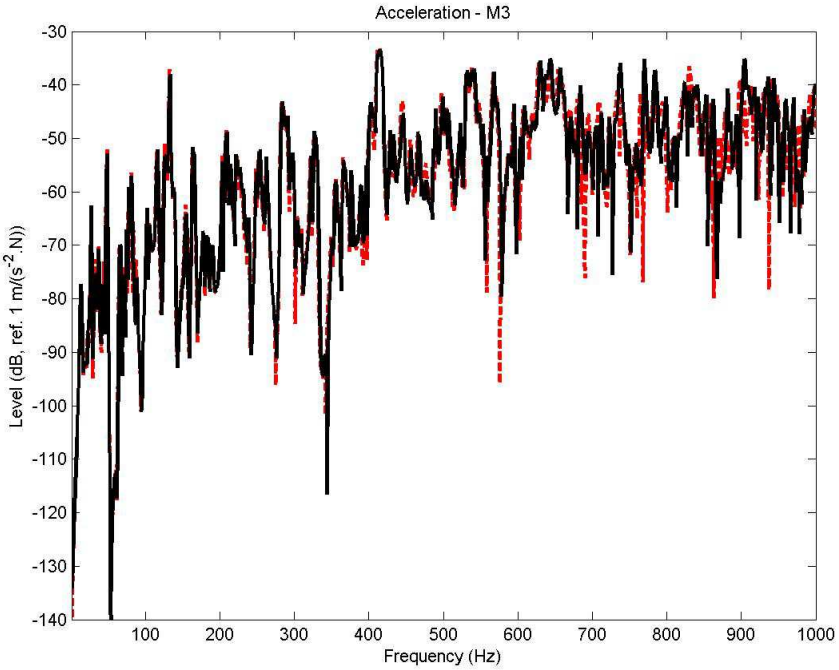

Figure 22. Comparison of the acceleration level at point M3 for two calculations: dashed line, PTF results; solid line, direct FEM results (reference).

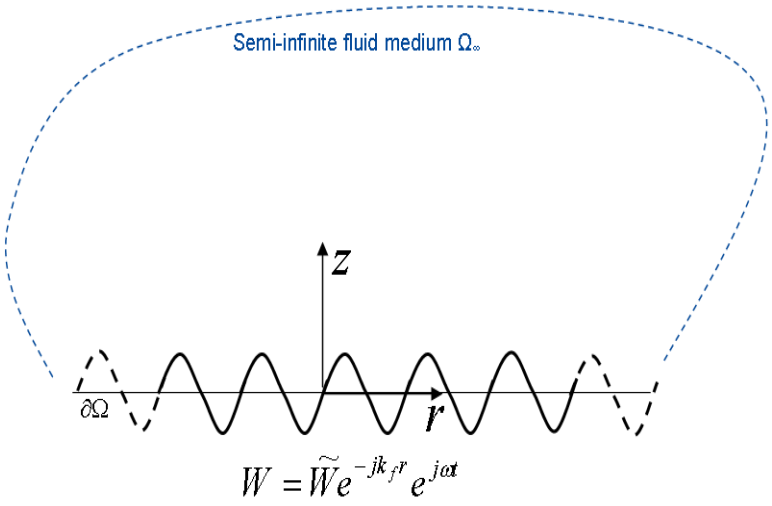

Figure 23. Semi-infinite 2D fluid medium with imposed displacements at the boundary.